

Supplementary Materials for

Hobit and Blimp1 instruct a universal transcriptional program of tissue residency in lymphocytes

Laura K. Mackay,* Martina Minnich, Natasja A. M. Kragten, Yang Liao, Benjamin Nota, Cyril Seillet, Ali Zaid, Kevin Man, Simon Preston, David Freestone, Asolina Braun, Erica Wynne-Jones, Felix M. Behr, Regina Stark, Daniel G. Pellicci, Dale I. Godfrey, Gabrielle T. Belz, Marc Pellegrini, Thomas Gebhardt, Meinrad Busslinger, Wei Shi, Francis R. Carbone, Rene A. W. van Lier, Axel Kallies,* Klaas P. J. M. van Gisbergen*

*Corresponding author. E-mail: lkmackay@unimelb.edu.au (L.K.M.); kallies@wehi.edu.au (A.K.); k.vangisbergen@sanquin.nl (K.P.J.M.v.G.)

Published 22 April 2016, *Science* **352**, 459 (2016)

DOI: 10.1126/science.aad2035

This PDF file includes

Materials and Methods
Figs. S1 to S17
References

Materials and Methods:

Mice

Zfp683^{-/-} (*Hobit* KO; (2)), *Prdm1* ^{GFP/+} (*Blimp1-GFP*; (31)), *Prdm1*^{flox/flox} x Lck Cre (*Blimp1* KO; (3)), *Prdm1*^{Bio/Bio} x Rosa26-^{BirA/BirA} (*Blimp1-Bio*; (32)), CAGs-rtTA3 mice (33), *Tbx21^{-/-}* (*T-bet* KO; (34)) and *Il15^{-/-}* (*Il15* KO; (35)) mice were maintained on a C57Bl/6 background. *Blimp1* KO were crossed onto *Hobit* KO mice to generate *Blimp1* × *Hobit* DKO mice. gBT-I mice are CD8⁺ TCR transgenic mice that recognize the H-2K^b-restricted HSV-1 gB epitope of amino acids 498-505 (gB₄₉₈₋₅₀₅). For the generation of mixed bone marrow (BM) chimeric mice, B6.SJL-Ptprc^aPep3^b/BoyJ (Ly5.1) or B6.SJL-Ptprc^aPep3^b/BoyJ × C57Bl/6 (Ly5.1 × Ly5.2) were used as recipients. Following irradiation (2 × 550 Rads), recipient mice were reconstituted by intravenous transfer of 2 × 10⁷ BM cells. Recipients were used in experiments 8-12 weeks after reconstitution. Chimerism was analyzed in the blood prior to experiments using flow cytometry using the congenic markers Ly5.1 and Ly5.2 to establish the relative size of host and donor compartments. The ratio between donor compartments within the blood prior to infection was used to calibrate the ratio of the indicated lymphocyte populations within experiments. Mice were maintained under SPF conditions and animal experiments were performed according to national and institutional guidelines.

Viral infections

Mice were infected with 1 × 10⁶ plaque forming units (PFU) of HSV type 1 by epicutaneous application after scarification, as described (28) or with 30 PFU of LCMV (strain WE) by intravenous injection. Infected mice were sacrificed at the indicated time points after infection and organs were harvested for analysis by flow cytometry.

Cell preparation

Single cell preparations of thymus, spleen, kidney and liver were obtained by passing organs over cell strainers (70 µM, BD Biosciences). Kidney and liver lymphocytes were isolated after resuspension of cell preparations in 44% Percoll (GE Healthcare) and density gradient centrifugation. Contaminating erythrocytes were removed using red blood cell lysis buffer (155 mM NH₄Cl, 10 mM KHCO₃, 1 mM EDTA). Skin tissue (1.5 × 1 cm²) was removed from

the flank following hair removal using Veet depilation cream (Reckitt Bencksier). To separate epidermis from dermis, skin pieces were digested in dispase (2.5 mg/ml) at 37°C for 1.5 h. To obtain single cell suspensions, the epidermis was digested in trypsin (0.25%) and EDTA (0.1%) at 37°C for 30 min and dermis in collagenase type III (3 mg/ml) and DNase I (5 ug/ml) at 37°C for 30 min. Single cell suspensions of epidermis and dermis were pooled and sequentially passed over 70 µm and 30 µm nylon mesh. Intraepithelial lymphocytes (IELs) and lamina propria lymphocytes (LPLs) were isolated from small intestine. After removal of associated fat tissue, Payers patches and fecal content, 1 cm² pieces of small intestine were incubated at 37°C for 30 min in Ca²⁺ and Mg²⁺ Free Hanks buffer containing 5 mM EDTA and 1mM DTT. IELs were isolated from the released epithelial fraction after resuspension in 44% Percoll, layering on top of 70% Percoll and density gradient centrifugation. LPLs were obtained after digestion of the remaining gut tissue in 1 mg/ml collagenase type III, 0.4 U/ml dispase and 100 µg/mL DNase at 37°C for 45 minutes.

Antibodies and Flow cytometry

Single cell suspensions were labeled with the indicated fluorescently conjugated antibodies at 4°C for 30 min in PBS containing 0.5% FCS. Tetramer labeling was performed at room temperature. Antibody and tetramer binding was analyzed on Canto or Fortessa (BD Biosciences) flow cytometers. The following antibodies were purchased from eBioscience, BD Biosciences or BioLegend: CD3 (145-2C11), CD4 (GK1.5), CD8 (53-6.7), CD24 (M1/69), CD49a (Ha31/8), CD49b (DX5), CD62L (MEL-14), CD69 (H1.2F3), CD103 (2E7), CD122 (TM-BETA1), CD127 (A7R34), CCR7 (4B12), CXCR6 (221002), Eomes (DAN11MAG), Granzyme B (GB11), IFN-γ (XMG1.2), KLRG1 (2F1), Ly5.1 (A20), Ly5.2 (104), NK1.1 (PK136), NKp46 (29A1.4), T-bet (4B10), TCRβ (H57-597), TNF-α (MP6-XT22), and TRAIL (N2B2). PBS57-loaded and vehicle-loaded CD1d tetramers were obtained from the tetramer core facility of the NIH; gB-loaded tetramers were generated in the Dept of Microbiology and Immunology, University of Melbourne, and gp33- and np396-loaded tetramers were obtained from BD Biosciences.

CD8 T cell cultures

CD8 T cells were isolated from spleen and lymph nodes using CD8 microbeads (Miltenyi) and magnetic sorting on LS columns (Miltenyi). Isolated CD8 T cells were stimulated with plate-

bound anti-CD3 antibodies (5 µg/ml) in the presence of anti-CD28 (2 µg/ml) and IL-2 (100 U/ml). CD8 T cells were expanded further in medium containing only IL-15 (20 ng/ml), IL-2 (100 U/ml) or IL-2 and IL-12 (5 ng/ml), as indicated. For analysis of *Hobit* and *Blimp1* expression in CD8 T cells, anti-CD3 and anti-CD28 stimulated T cells were cultured for 7 days in the presence of IL-2, and then cultured in medium containing the following cytokines for a further 24 hr: IL-15/IL-15-antibody complexes (50 ng/ml IL-15 and 250 ng/ml IL-15R α) or TGF β (5 ng/ml). For retroviral transduction experiments, activated CD8 T cells were transduced with retroviruses overexpressing T-bet or Eomes (or control empty retrovirus), as previously described (17).

NKT cell cultures

Single cell preparations of thymus were enriched for NKT cells using magnetic depletion of CD8+ and CD24+ thymocytes with anti-CD8 and anti-CD24 antibodies and goat anti-rat beads (Qiagen). NKT cells were isolated using cell sorting with anti-TCR β antibodies and PBS57-loaded CD1d tetramers. Isolated NKT cells were stimulated with plate-bound anti-CD3 antibodies (5 µg/ml) in medium containing anti-CD28 (2 µg/ml) and IL-2 (100 U/ml). Expanded NKT cells were re-plated after 3 days in medium containing IL-15 (20 ng/ml) and cultured for an additional 7 days.

T cell transfers

For experiments using transgenic gBT-I cells, adoptive transfers of naïve gBT-I cells were carried out intravenously with lymph node suspensions (5×10^4 cells) prior to HSV infection. To study the effect of IL-15, WT and *Il15* KO mice were infected with HSV and 4 days later received effector gBT-I cells ($5-12 \times 10^4$ cells) enriched from the spleens of WT mice 6 days after HSV infection. For experiments where CD8 T cells were transferred by intradermal injection, *in vitro* expanded CD8 T cells (1×10^6 cells) were injected into the skin (five 20-µl injections over an area of skin 1×1.5 cm 2) using a 30-gauge needle, as described (9). For adoptive transfer experiments with NKT cells, *in vitro* expanded NKT cells (1×10^6 cells) were transferred by intravenous injection. Recipient mice were sacrificed at the indicated time points.

Quantitative PCR and Taqman

To perform qPCR analysis, RNA was isolated using RNeasy Mini Kit according to the manufacturer's instructions (Qiagen). RNA was synthesized into cDNA using iScript cDNA Synthesis Kit (BioRad). qPCR was run on a C1000 Thermal Cycler (BioRad) using Sensimix SYBR No ROX Kit (Bioline). The following primer pairs were used: *Hobit* (forward: 5'-CTCAGCCACTTGCAGACTCA-3', reverse: 5'-CTGTCGGTGGAGGCTTGTA-3'), *Blimp1* (forward: 5'-TTCTCTTGGAAAAACGTGTGGG-3', reverse: 5'-GGAGCCGGAGCTAGACTTG-3'), *S1pr1* (forward: 5'-GTGTAGACCCAGAGTCCTGCG-3', reverse: 5'-AGCTTTCCCTGGCTGGAGAG-3'), *Klf2* (forward: 5'-CTCAGCGAGCCTATCTGCC-3', reverse: 5'-CACGTTGTTAGGTCCATCC-3'), *Ccr7* (forward: 5'-GGGTTCCCTAGTGCCTATGCTGGCTATG-3', reverse: 5'-GGCAATGTTGAGCTGCTGGTT-3'), and *Hprt* (forward: 5'-GGGGGCTATAAGTTCTTGC-3', reverse: 5'-TCCAACACTTCGAGAGGTCC-3'). Expression was normalized using *Hprt* and the expression was quantified relative to expression in total or naïve WT CD8 T cells set to 1. The expression of *Hobit* and *Blimp1* in gBT-I cells after HSV infection was analysed using Taqman assay. RNA extraction, cDNA synthesis, preamplification and quantitative RT-PCR were performed using Taqman Gene Expression Cells-To-Ct Kit, Taqman Fast Preamp master mix and assorted commercially available Taqman assays (Mm00437762_m1, Mm00446973_m1, Mm00446968_m1, Mm00476128_m1) with Taqman Fast Advanced Mastermix on a StepOnePlus Real-Time PCR cycler (Life Technologies). To perform Taqman on *Hobit* the following probe was used in combination with the qPCR primers of Hobit: 6-FAM-5'-TCATGACTTAGCCTGGAGCGAGAGGATGT-3'-TAMRA. The threshold cycle of respective genes for each cell population was normalized to the arithmetic mean of *Hprt*, *B2m* and *Tbp* housekeeping genes (DCt). Normalized gene expression of each cell type was compared to the gene expression of naïve gBT-I cells (set to 1) according to the 2(-DDCT) method.

RNA-sequencing

LCMV-specific CD8 T cell populations were isolated by flow cytometric sorting from LCMV-infected mice at day 40+ post-infection using gp33 and np396 tetramers. Following HSV infection (day 40+) gBT-I cells were isolated by sorting on Vα2+CD45.1+ cells. Tcm (CD62L+CD69-) and Tem (CD62L-CD69-) populations were obtained from the spleen. LCMV-specific Tem were also obtained from the liver. CD103+ Trm populations (CD69+CD103+)

were obtained from skin after HSV infection and the intraepithelial fraction of the small intestine after LCMV infection. LCMV-specific CD103⁺ Trm (CD62L⁺CD69⁺) populations were isolated from liver. Splenic naïve CD8 T cells (CD8⁺CD44⁺CD62L⁺) and liver-derived NKT cells (CD3⁺CD1d-PBS57 tetramer⁺), trNK cells (CD3⁻NK1.1⁺NKp46⁺CD49a⁺CD49b⁻) and cNK cells (CD3⁻NK1.1⁺NKp46⁺CD49a⁺CD49b⁺) were isolated from WT mice under homeostatic conditions. To establish the role of Hobit and Blimp-1, NKT cells (TCR^b+CD1d-PBS57 tetramer⁺) were sorted to purity from NKT cell cultures, established as described above. RNA purification was performed following the manufacturer's protocol using the RNAeasy Plus Mini Kit (Qiagen). RNA samples were sequenced on an Illumina HiSeq analyzer, producing between 13 and 33 million 100-bp single-end reads per sample. Two or more biological replicates were generated and sequenced for each sample. Sequence reads were aligned to the GRCm38/mm10 build of the *Mus musculus* genome using the Subread aligner (36). Only uniquely mapped reads were retained. Genewise counts were obtained using featureCounts (37). Reads overlapping exons in annotation build 38.1 of NCBI RefSeq database were included. Genes were filtered from downstream analysis if they failed to achieve a CPM (counts per million mapped reads) value of at least 1 in at least two libraries. Counts were converted to log₂ counts per million, quantile normalized and precision weighted with the 'voom' function of the limma package (38, 39). A linear model was fitted to each gene, and empirical Bayes moderated *t*-statistics were used to assess differences in expression (40). Genes were called differentially expressed if they achieved a false discovery rate (FDR) of 0.05 or less and had an expression change of >1.5 fold or >2 fold, as indicated. The called differentially expressed genes must also have at least 4 or 8 RPKMs (reads per kilobase of exon length per million mapped reads) in one or both of the two cell types being compared, as indicated. The gene set enrichment plots were generated with the 'barcodeplot' function in limma. Gene set enrichment analysis was carried out using the 'roast' method in limma with 999 rotations (41). One-sided P values are reported.

Habit ChIP

For retroviral transduction experiments, we cloned full-length mouse Hobit cDNA with a N-terminal V5-tag into a pSIN retroviral vector (pSIN-TRE3G-V5-mHabit-P2A-GFP). Tet-inducible V5-tagged Hobit expression was driven by the TRE3G promoter and followed by P2A-GFP. The retrovirus was produced using retroviral helper plasmid (pCMV-Gag-Pol, Cell

Biolabs) into Platinum-E (Cell Biolabs) packaging cells using calcium phosphate transfection in the presence of chloroquine (25 µM). Viral supernatant was collected at 24-36 hr after transfection and passed through a 0.45-µm filter. Tet-on competent CD8 T cells were isolated from the spleen and lymph nodes of CAGs-rtTA3 mice and stimulated with anti-CD3, anti-CD28 and IL-2 (100 U/ml) for 3 days. To establish transduction, the activated CD8 T cells were centrifuged 3 times at 8 hr-intervals in the presence of viral supernatant and polybrene (4 µg/ml) at 2,000 rpm for 30 min. The transduced CD8 T cells were further stimulated with IL-2 and IL-12 (5 ng/ml) for another 2 days together with doxycycline (1 µg/ml) to induce Hobit expression. Transduced cells were sorted based on GFP expression with a FACS Aria machine (Becton Dickinson) and subjected to chromatin precipitation with anti-V5 agarose (clone V5-10, Sigma). Briefly, 70×10^7 cells were fixed with 1% formaldehyde for 10 min followed by quenching with 0.125 M glycine for 5 min. The cells were lysed in 0.25% SDS buffer for 1 hr. The released chromatin was sheared to an average size of 500 bp using a Biorupter™ sonicator (Diagenode). After removal of cell debris, the chromatin (400 µg) was diluted in buffer containing 1% Triton and pre-cleared using Protein G Plus agarose (Santa Cruz Biotechnology). The pre-cleared chromatin was incubated overnight at 4°C with anti-V5 agarose. After washing, the Hobit-V5 binding protein-DNA complexes were eluted using buffer containing 1% SDS and 100 mM NaHCO₃. Reverse cross-linking was performed on the eluates with buffer containing 10 mM Tris-HCl (pH 8.0), 1 mM EDTA and 200 mM NaCl in the presence of proteinase K (500 g/ml). Genomic DNA was isolated from the precipitated material by phenol extraction and ethanol precipitation. The precipitated genomic DNA was quantified by real-time PCR.

Blimp1 ChIP

Splenic CD8 T cells from *Blimp1*-Bio mice were stimulated first with anti-CD3, anti-CD28 and IL-2 (100 U/ml) for 3 days and then with IL-2 and IL-12 (5 ng/ml) for another 2 days. *Blimp1*-Bio mice carry a biotin acceptor sequence at the carboxyl terminus of Blimp1, which was biotinylated *in vivo* by coexpression of the Escherichia coli biotin ligase BirA from the Rosa26^{BirA} allele. Chromatin from $\sim 3 \times 10^8$ CD8 T cells was prepared using a lysis buffer containing 0.25% SDS prior to chromatin precipitation by streptavidin pulldown (Bio-ChIP), as described (42). The precipitated genomic DNA was quantified by real-time PCR.

ChIP-sequencing

Approximately 1-5 ng of ChIP-precipitated DNA was used as starting material for the generation of sequencing libraries with the NEBNext Ultra Ligation Module and NEBNext End Repair/dA-Tailing module. DNA fragments of 200–500 bp were selected with AMPure XP beads (Beckman Coulter). PCR amplification was performed with the KAPA Real Time Amplification kit (KAPA Biosystems). Completed libraries were quantified with the Agilent Bioanalyzer dsDNA 1000 assay kit and Agilent QPCR NGS Library Quantification kit. Cluster generation and sequencing was carried out by using the Illumina HiSeq 2000 system with a read length of 50 nucleotides according to the manufacturer's guidelines. Sequence reads that passed the Illumina quality filtering were considered for alignment. Reads were aligned to the mouse genome assembly version of July 2007 (NCBI37/mm9) using bowtie version 1.0.0. For peak calling of ChIP-seq data we used the MACS program version 1.3.6.1 with default parameters, a genome size of 2,654,911,517 bp (mm9) and a mixture of pro-B and mature B cell input control sample. Peaks were filtered for P values of $< 10^{-7.5}$. Peaks were assigned to target genes, as described (43).

Peak-overlap and motif analysis

The Multovl program (44) was used for the peak overlap analysis. The minimal overlap length was set to one. Motif analyses were performed with the Gimme-Motifs program (45) with default settings for *de novo* Blimp1 and Hobit motif prediction from the top 250 peaks of each data set.

Migration assays

Migration assays were performed with cultured thymic NKT cells using 24-well plates with transwell inserts (5 μ m pores, Costar). The chemo-attractants CCL21 (R & D Systems) or S1P (Sigma) were added to the lower chamber. NKT cells were allowed to migrate for 3 h at 37°C. Migrated NKT cells were enumerated using counting beads on a flow cytometer. NKT cell migration was calculated as the ratio of migrated cells relative to control conditions without chemo-attractants.

Immunofluorescence staining and confocal microscopy

Spleens were cut in small pieces and incubated in 40 µg/mL CD1d-PBS57 or vehicle-loaded PE-labelled tetramer in PBS 2% FCS for 18 h at 4°C. Spleens were washed in PBS and fixed in 4% PFA for 1 h on ice, then washed in PBS, dehydrated in 30% sucrose and frozen in OCT (Sakura, Finetek). Spleen sections were cut on a cryostat at 10 µm, and stained using B220-Pacific Blue and CD3-eFluor660 (eBiosciences). PE-labelled tetramer was detected using a polyclonal rabbit-anti-PE antibody (Novus Biologicals), followed by an anti-rabbit Alexa Fluor 555 antibody (Life Technologies). Sections were mounted using Prolong Gold Antifade (Life Technologies) and imaged on a Zeiss LSM710 confocal microscope. Image files were processed using Imaris 7.5 (Bitplane).

Statistical analysis

Values are expressed as mean ± S.E.M. Differences between two groups were assessed by Student's t test and differences between more than two groups were assessed using one-way ANOVA followed by a Bonferroni post-hoc test. After log₂ transformation ratios were compared to 0 by one-sample Student's t test. A p-value of less than 0.05 was considered statistically significant. * denotes $P < 0.05$, ** denotes $P < 0.01$ and *** denotes $P < 0.001$.

Supplementary Figure Legends:

Figure S1: Hobit and Blimp1 are co-expressed in LCMV-specific Trm. (A) *Hobit* and (B) *Blimp1* expression was determined by qPCR in LCMV-specific central memory (Tcm), effector memory (Tem) and tissue-resident memory CD8 T cells (Trm) from the intraepithelial lymphocyte fraction of the small intestine (SI IEL) at day 40+ after LCMV infection. Data in (A,B) represent pooled results of 3 mice per group. Bars denote mean ± S.E.M.

Figure S2: Hobit and Blimp1 are required for development of CD8 T cells with a Trm phenotype in skin. Activated congenically marked CD8 T cells from WT mice (Ly5.1/2+) were intradermally injected at a 1:1 ratio together with CD8 T cells from *Hobit* KO, *Blimp1* KO or *Blimp1* x *Hobit* DKO mice (Ly5.2+) into recipient mice (Ly5.1+). (A) Representative dot plots display WT and *Blimp1* x *Hobit* DKO donor CD8 T cell populations as detected by Ly5.1 and Ly5.2 expression in the spleen (top row) and skin (bottom row) at the indicated time-points after transfer. (B) Bar graph shows the ratio (log2) of transferred WT and *Blimp1* x *Hobit* DKO CD8 T cells in spleen, draining lymph node and skin at day 6 after transfer. (C) Representative histograms display CD69 (left) and CD103 (right) expression on donor WT (black line) and *Hobit* KO or *Blimp1* KO (grey filled) CD8 T cells 14-15 days post intradermal injection. Data in (A-C) are representative of 5-8 mice per group. *** P < 0.001 as determined by one-way ANOVA (B). Bars denote mean ± S.E.M.

Figure S3: Hobit and Blimp1 regulate effector CD8 T cell differentiation during HSV infection. (A,B) Mixed BM chimeric mice containing WT (Ly5.1+) hematopoietic cells together with WT control or *Blimp1* x *Hobit* DKO (Ly5.2+) cells were analyzed for virus-specific effector CD8 T cells in spleen at day 10-11 after infection with HSV. (A) Plots display expression of KLRG1 and CD127 on gB tetramer+ CD8 T cells in the WT and *Blimp1* x *Hobit* DKO compartments of mixed BM chimeric mice. (B) Bar graph displays the percentage of KLRG1+CD127- short-lived effector cells (SLEC) and KLRG1-CD127+ memory precursor effector cells (MPEC) within the gB tetramer+ CD8 T cell population. Data in (A,B) are

representative of two independent experiments with 3-4 mice per group. * $P < 0.05$ and *** $P < 0.001$ as determined by two-tailed Student's t test (B). Bars denote mean \pm S.E.M.

Figure S4: Blimp1, but not Hobit, regulates effector CD8 T cell differentiation during LCMV infection. Mixed BM chimeric mice containing WT (Ly5.1+) hematopoietic cells together with WT control, *Hobit* KO, *Blimp1* KO or *Blimp1* x *Hobit* DKO (Ly5.2+) cells were analyzed for virus-specific effector CD8 T cells in spleen at day 8-11 after infection with LCMV. (A) Plots display KLRG1 and CD127 expression on gp33 tetramer+ CD8 T cells of the indicated genotypes. (B) Bar graph displays the ratio (log2) between WT (Ly5.1+) and WT or mutant (Ly5.2+) compartments within SLEC and MPEC gp33 tetramer+ CD8 T cells. (C) Representative plots display the expression of granzyme B within WT (Ly5.2-) and the indicated WT or mutant (Ly5.2+) compartments of virus-specific CD8 T cells. (D) Expression of intracellular IFN- γ and TNF- α was determined in CD8 T cells of the indicated genotype following brief restimulation with gp33 peptide. (E-G) The percentage of CD8 T cells of the indicated genotype that displayed expression of (E) granzyme B, (F) IFN- γ , and (G) TNF- α was quantified. Data in (A,B) are the pooled results of two independent experiments with 3-7 mice per group. Data in (C-G) are representative of two independent experiments with 3 to 4 mice per group. ** $P < 0.01$ and *** $P < 0.001$ as determined by one-sample Student's t test (B) or by one-way ANOVA (E). Bars denote mean \pm S.E.M.

Figure S5: Hobit and Blimp-1 regulate the maintenance of gut-resident memory T cells after LCMV infection. Mixed BM chimeric mice with WT (Ly5.1+) and WT control, *Hobit* KO, *Blimp1* KO, or *Blimp1* x *Hobit* DKO (Ly5.2+) compartments were infected with LCMV to analyze the LCMV-specific CD8 T cell response within spleen and gut. (A) Representative flow cytometry plots display Ly5.1 and Ly5.2 expression of gp33 tetramer+ CD8 T cells from spleen, and intraepithelial and lamina propria fractions of the small intestine (SI IELs and SI LPLs, respectively) in mixed BM chimeric mice containing a WT (Ly5.1+) and *Blimp1* x *Hobit* DKO (Ly5.2+) compartment. (B) Bar graphs display the ratio (log2) of gp33+ CD8 T cells from Ly5.1+ WT and Ly5.2+ WT control or mutant compartments in the indicated tissues at day 10 (top row) and day 50+ (bottom row) after LCMV infection. Data are representative of two independent experiments with 3-4 mice per group. * $P < 0.05$, ** $P < 0.01$ and *** $P < 0.001$ as determined by one-sample Student's t test (B). Bars denote mean \pm S.E.M.

Figure S6: Hobit maintains tissue-resident NK cells in the liver. (A) Expression of Blimp1 was analyzed on tissue-resident NK cells (trNK) and conventional NK cells (cNK) in liver using GFP expression in heterozygous *Blimp1*-GFP reporter mice (black line) and WT controls (filled grey). (B) Representative plots display expression of CD49a and Eomes, CD69 and CD62L, TRAIL and CD49b, and CXCR6 and CD49b of total liver NK cells of WT (left panels) and *Hobit* KO mice (right panels). Data are representative of (A) three or (B) two independent experiments.

Figure S7: Hobit and Blimp1 regulate the Trm-phenotype of NKT cells. (A) Dot plots display expression of CD49a and CD69 on splenic NKT cells of the indicated genotypes. (B) The number of CD69- and CD69+ NKT cells was determined in spleens of WT, *Hobit* KO, *Blimp1* KO and *Blimp1* x *Hobit* DKO mice. (C) Expression of Blimp1 was analyzed on NKT cells in thymus, spleen and liver using GFP expression in heterozygous *Blimp1*-GFP reporter mice (black line) and WT controls (filled grey). Data in (A,B) are representative of three independent experiments with 6-11 mice per group. Data in (C) are representative of at least three independent experiments. * $P < 0.05$ and *** $P < 0.001$ as determined by one-way ANOVA (B). Bars denote mean \pm S.E.M.

Figure S8: The maintenance of NKT cells in the liver but not the spleen depends on Hobit and Blimp1. (A) Representative flow cytometry plots display the binding of anti-TCR β antibodies and PBS57-loaded CD1d tetramers to total splenocytes (top panel) and total liver lymphocytes (bottom panel) from WT, *Hobit* KO, *Blimp1* KO and *Blimp1* x *Hobit* DKO mice. (B) Plots display the binding of anti-Ly5.1 antibodies and PBS57-loaded CD1d tetramers to total donor splenocytes (top panel) and total donor liver lymphocytes (bottom panel) in mixed BM chimeric mice containing control WT (Ly5.1+) and WT, *Hobit* KO, *Blimp1* KO or *Blimp1* x *Hobit* DKO compartments (Ly5.2+). Results represent pooled data of three (A) or four (B) different experiments with 6-11 mice per group.

Figure S9: Hobit and Blimp1 co-regulate maintenance of liver but not splenic NKT cells. (A) Congenically marked NKT cells of WT or *Blimp1* x *Hobit* DKO mice (Ly5.2+) were co-transferred together with competitor WT NKT cells (Ly5.1+) into WT recipients (Ly5.1/2+) in

a 1:1 ratio. Representative dot plots display WT and *Blimp1* x *Hobit* DKO donor NKT cell populations as detected by Ly5.1 and Ly5.2 expression in the liver at indicated time points after transfer. (B) Bar graph displays the ratio (log2) between Ly5.1+ and Ly5.2+ donor NKT cells. (C) The ratio (log2) between WT (Ly5.1+) and WT, *Hobit* KO, *Blimp1* KO and *Blimp1* x *Hobit* DKO mice (Ly5.2+) donor NKT cells was determined in spleen (left) and liver (right) at day 15+ post transfer. (D) Histograms display CTV dilution of donor NKT cells of WT and *Blimp1* x *Hobit* DKO mice. (E) The division index of donor NKT cells of WT and *Blimp1* x *Hobit* DKO mice was calculated. Results are representative of two independent experiments with 3 mice per group. * $P < 0.05$, ** $P < 0.01$ and *** $P < 0.001$ as determined by two-tailed Student's *t* test (B) or by one-sample Student's *t* test (C). Bars denote mean ± S.E.M.

Figure S10: LCMV-specific CD69+ CD8 T cells in liver and kidney display a Trm phenotype and require Hobit and Blimp1. Antigen-specific CD8 T cells were analyzed in WT mice using gp33 tetramer at day 40+ after infection. (A) The percentage of CD62L-CD69+ Trm within the LCMV-specific CD8 T cell population was quantified in blood and liver. (B-D) Expression of (B) *S1pr1*, (C) *Klf2* and (D) *Ccr7* as determined by qPCR in the indicated populations of LCMV-specific CD8 T cells in spleen and liver. (E,F) Expression of (E) *Hobit* and (F) *Blimp1* as determined in the indicated populations of naïve CD8 T cells and LCMV-specific gp33+ CD8 T cells using qPCR. Short-lived effector cells (KLRG1+CD127-, SLEC) and memory-precursor effector cells (KLRG1-CD127+, MPEC) were analyzed at day 8, and Tcm (CD62L+CD69-), Tem (CD62L-CD69-), and Trm (CD62L-CD69+) were analyzed at day 30+ after infection with LCMV. (G,H) LCMV-specific CD8 T cells were analyzed within the kidney of mixed BM chimeric mice containing control WT (Ly5.1+) and WT, *Hobit* KO, *Blimp1* KO, or *Blimp1* x *Hobit* DKO (Ly5.2+) compartments at day 50+ following infection with LCMV. (G) Expression of CD69 and CD103 was determined on gp33 tetramer+ CD8 T cells of the indicated genotype. (H) Bar graph displays the ratio of CD69+ LCMV-specific CD8 T cells from WT (Ly5.1+) and WT or mutant (Ly5.2+) compartments within kidney. Results represent 3-6 samples of two independent experiments. * $P < 0.05$ and ** $P < 0.01$ as determined by two-tailed Student's *t* test (A) or by one-way ANOVA (H). Bars denote mean ± S.E.M.

Figure S11: Hobit expression is regulated by IL-15 and T-bet. (A) *Hobit* (left) and *Blimp1* (right) expression in adoptively transferred WT gBT-I cells sorted from skin of WT or *Il15* KO

mice at day 14 after HSV infection, as determined by Taqman qPCR. (B) Activated WT and *T-bet* KO CD8 T cells were incubated with IL-15/IL-15-antibody complexes, TGF β or without stimuli (control) for 24 hr. *Hobit* expression in the cultured CD8 T cells was examined using qPCR. (C) Similarly, *Hobit* expression was determined in activated CD8 T cells transduced with overexpression vectors for T-bet and Eomes or with empty vector (control). Results in (A-C) are presented as mean values relative to expression in WT CD8 T cells. Data in (A) represents 10 mice per group and data in (B,C) is representative of 2-4 independent experiments. Bars denote mean \pm S.E.M.

Figure S12: NKT1 in contrast to NKT2 display characteristics of tissue-resident lymphocytes. (A) Thymic NKT cells of WT Balb/c mice were identified through binding of CD1d tetramers and anti-CD3 antibodies. Surface expression of CD122 was used to separate the NKT1 and NKT2 populations. (A) Representative histograms show expression of T-bet (left) and CD69 (right). (B) The geometric mean fluorescence intensity (geo MFI) of CD69 expression was quantified. (C) Thymic NKT1 and NKT2 cells were sorted from Balb/c mice using CD1d tetramers, anti-CD3 antibodies and anti-CD122 antibodies. Expression of *Hobit*, *Blimp1*, *S1pr1* and *Ccr7* was determined using qPCR. Data in (A-C) are representative of two independent experiments with 3 to 4 mice per group. * $P < 0.05$ and *** $P < 0.001$ as determined by two-tailed Student's *t* test (B,C). Bars denote mean \pm S.E.M.

Figure S13: Liver Trm are distinct from splenic and liver Tem and share characteristics with epithelial Trm. HSV-specific and LCMV-specific Tcm, Tem and Trm populations of spleen, liver, skin and the intraepithelial fraction of the small intestine (SI IEL) were isolated and analyzed using RNA-sequencing. (A) Heatmap displays the expression profile of genes associated with HSV-specific skin Trm and LCMV-specific gut Trm in the indicated populations of virus-specific CD8 T cells. Relative expression levels (Z-scores) of genes are shown, color-coded according to the legend. Rows are scaled to have a mean of 0 and an s.d. of 1. (B) Differentially expressed (DE) genes (FDR < 0.05 , fold change >2 , and RPKM >8) in pairwise comparisons of LCMV-specific Tem from spleen and liver, and liver Trm were enumerated. Number of upregulated (black bars) and downregulated genes (white bars) are displayed separately. (C) DE genes were determined between HSV-specific Trm (skin) or LCMV-specific Trm (liver and gut) and corresponding virus-specific Tcm and Tem subsets

from spleen and liver in pairwise comparisons. Numbers in overlapping parts of the Venn diagram indicate gene transcripts that overlap between Trm populations and numbers in unique parts of the Venn diagram display tissue-specific gene transcripts. (D) Enrichment of the set of 192 genes associated with epithelial Trm was analyzed in LCMV-specific liver Trm compared to liver Tem. The horizontal axis shows empirical Bayes moderated t-statistics for all genes comparing liver Trm to liver Tem and the vertical bars show the ranks of the up- and downregulated epithelial Trm signature genes. Up- and downregulated genes are shown in red and blue, respectively. Red and blue worm lines show enrichment of up- and down-regulated signature genes relative to random ordering. Roast P values for enrichment of up- and downregulated signature genes are < 0.001 . RNA-sequencing data are pooled from two independent experiments.

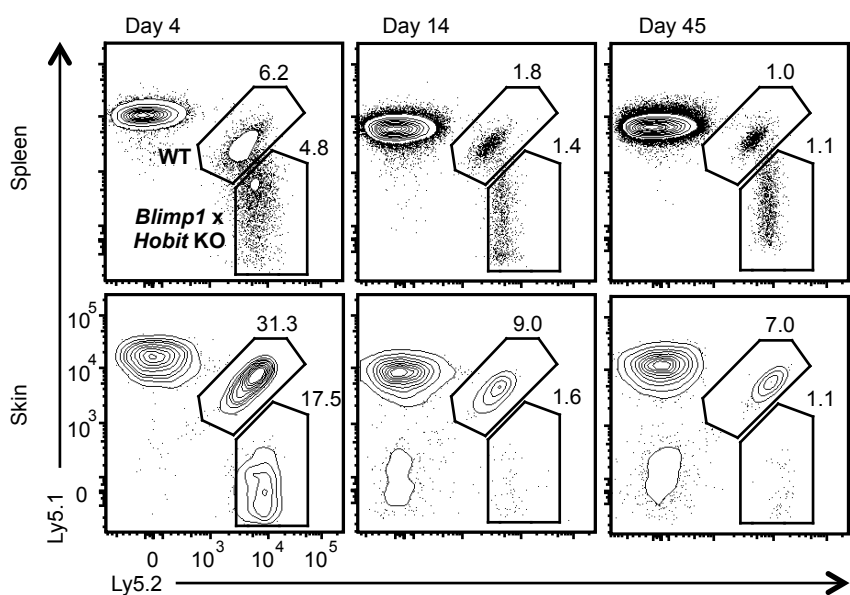
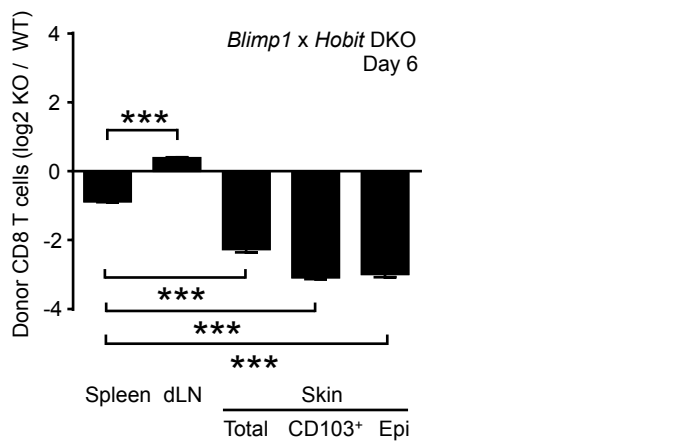
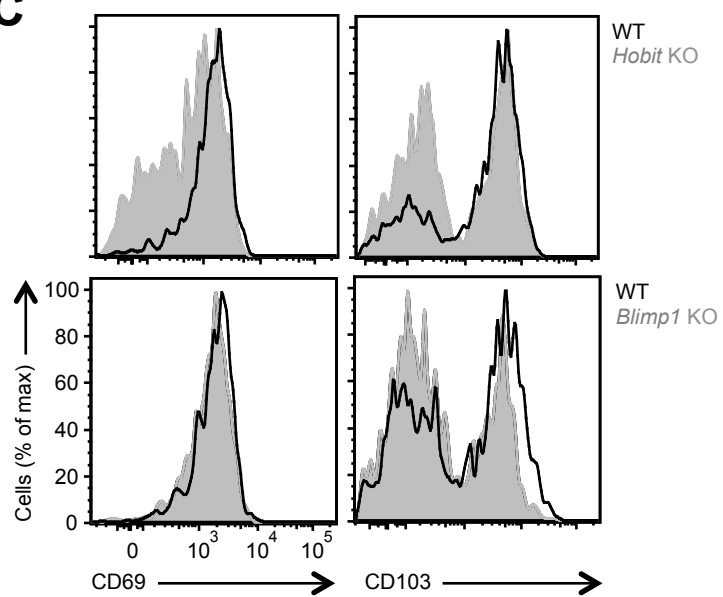
Figure S14: The gene signature of epithelial Trm is enriched in innate tissue-resident lymphocytes. (A) The 192 epithelial Trm signature genes associated with virus-specific Trm from skin and gut after HSV and LCMV infection, respectively, were overlaid with differentially regulated gene transcripts in pairwise comparative analysis of liver-derived cNK with trNK and of liver-derived Tem with NKT cells. Numbers in overlapping parts of the Venn diagram indicate gene transcripts that overlap between adaptive and innate tissue-resident populations and numbers in unique parts of the Venn diagram display specific gene transcripts of Trm, trNK and NKT cells. (B,C) Gene set enrichment tests show that epithelial Trm signature genes are significantly enriched in (B) trNK compared to cNK cells and in (C) NKT cells compared to liver-derived Tem. Universally upregulated and downregulated genes in epithelial Trm are shown in red and blue vertical bars, respectively. Roast P values for enrichment of up- and downregulated genes in (B,C) are < 0.001 . RNA-sequencing data are pooled from two independent experiments.

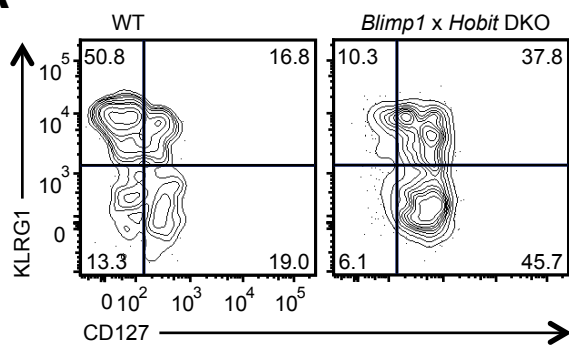
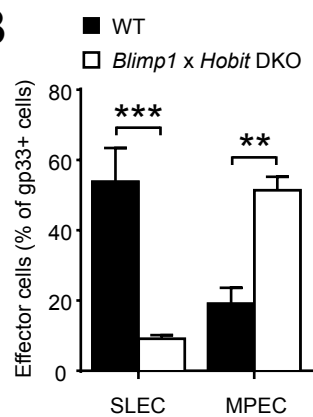
Figure S15: Cultured NKT cells maintain expression of the tissue-residency-associated molecule CD69 in a Hobit and Blimp1-dependent manner. Thymic NKT and splenic CD8 T cells were stimulated with anti-CD3, anti-CD28 and IL-2 for 3 days and further expanded in IL-15 for another 7 days. (A) Expression of Hobit and Blimp1 was analyzed in cultured NKT cells and CD8 T cells of WT mice using qPCR. (B) Expression of CD69 was analyzed on cultured NKT cells of WT, *Hobit* KO, *Blimp1* KO or *Blimp1* × *Hobit* DKO mice using flow

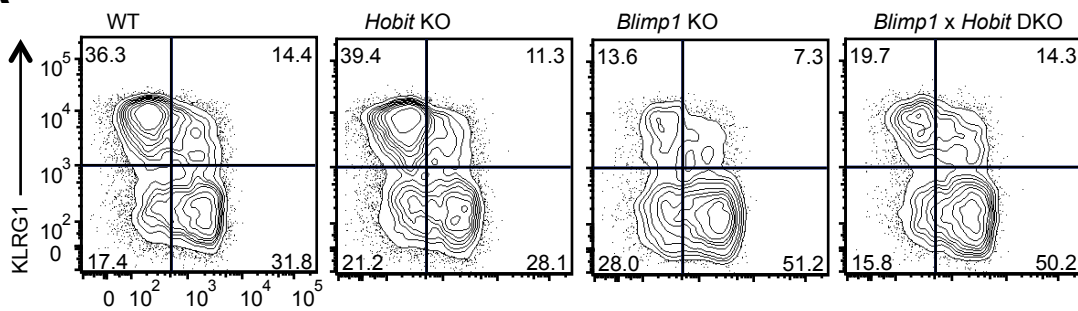
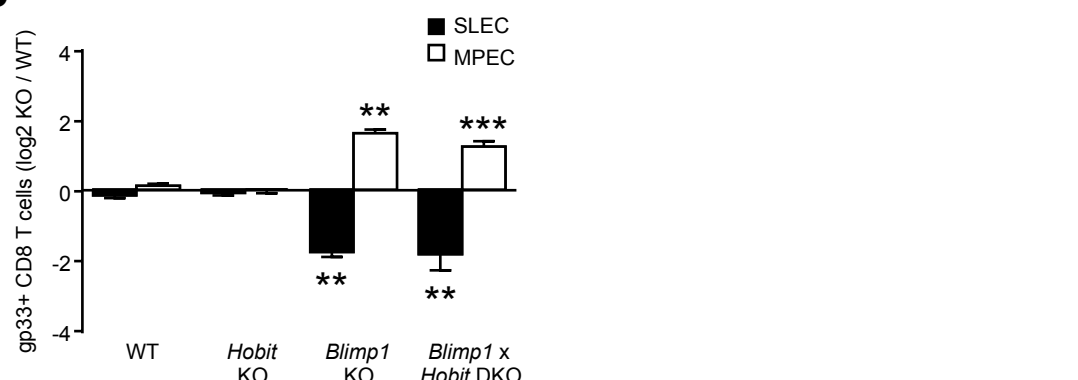
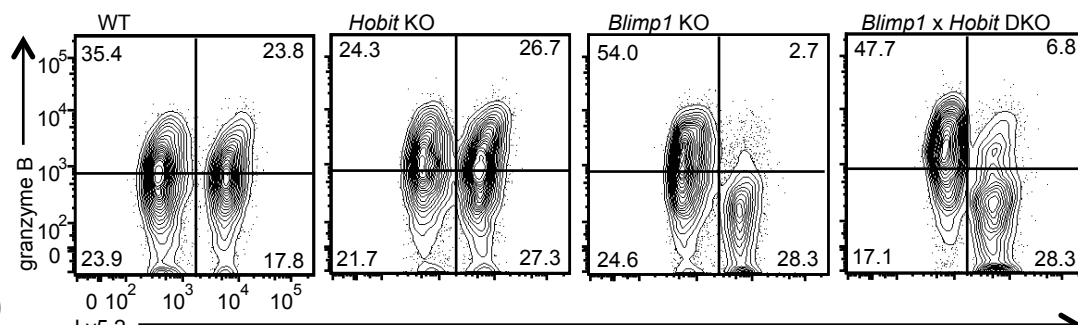
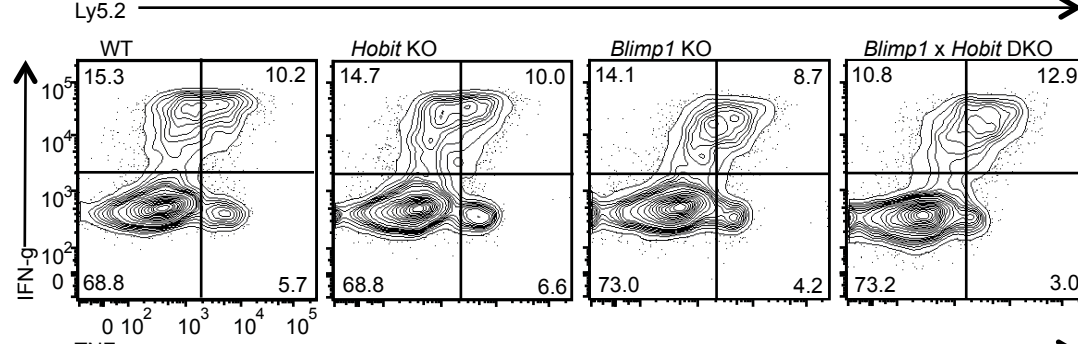
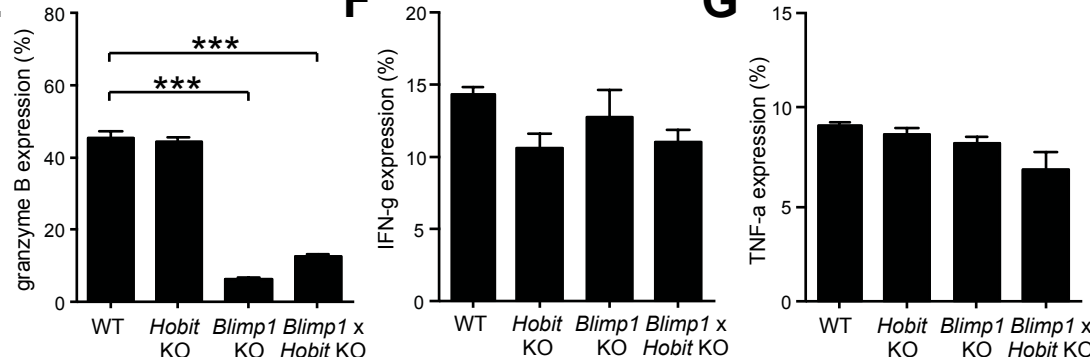
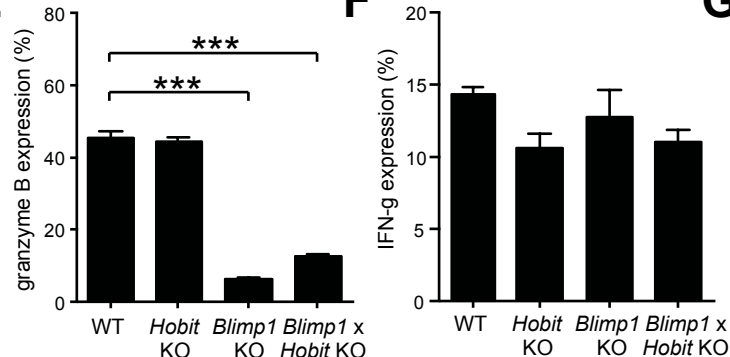
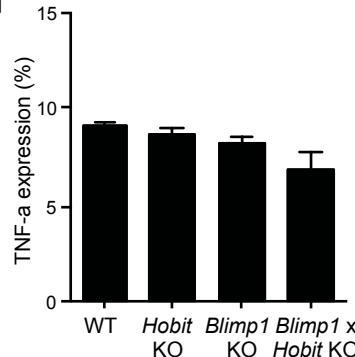
cytometry. Histograms display expression of CD69 on NKT cells of WT mice (black line) overlaid with that of the indicated KO mice (filled grey). (C) Gene set enrichment graph shows that the 30 genes associated with tissue-resident lymphocytes are significantly enriched in WT compared to *Blimp1* x *Hobit* DKO NKT cells. Vertical bars display the ranks of the tissue-residency signature genes. Upregulated and downregulated genes in tissue-resident lymphocytes are shown in red and blue vertical bars, respectively. Worm line shows enrichment score of upregulated (red lines) and downregulated tissue-residency signature genes (blue lines) relative to random ordering. Roast *P* values for enrichment of up- and downregulated genes are < 0.001. Data are representative of three independent experiments. Bars denote mean ± S.E.M.

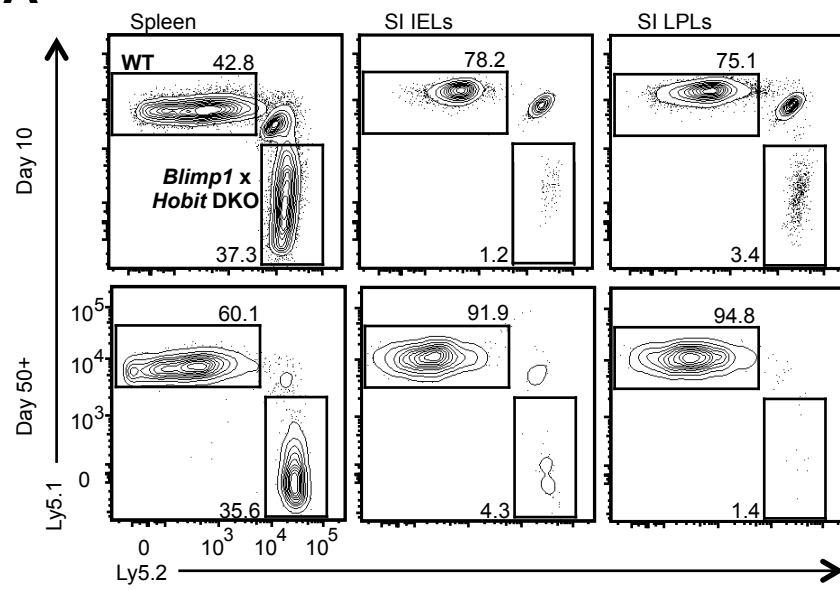
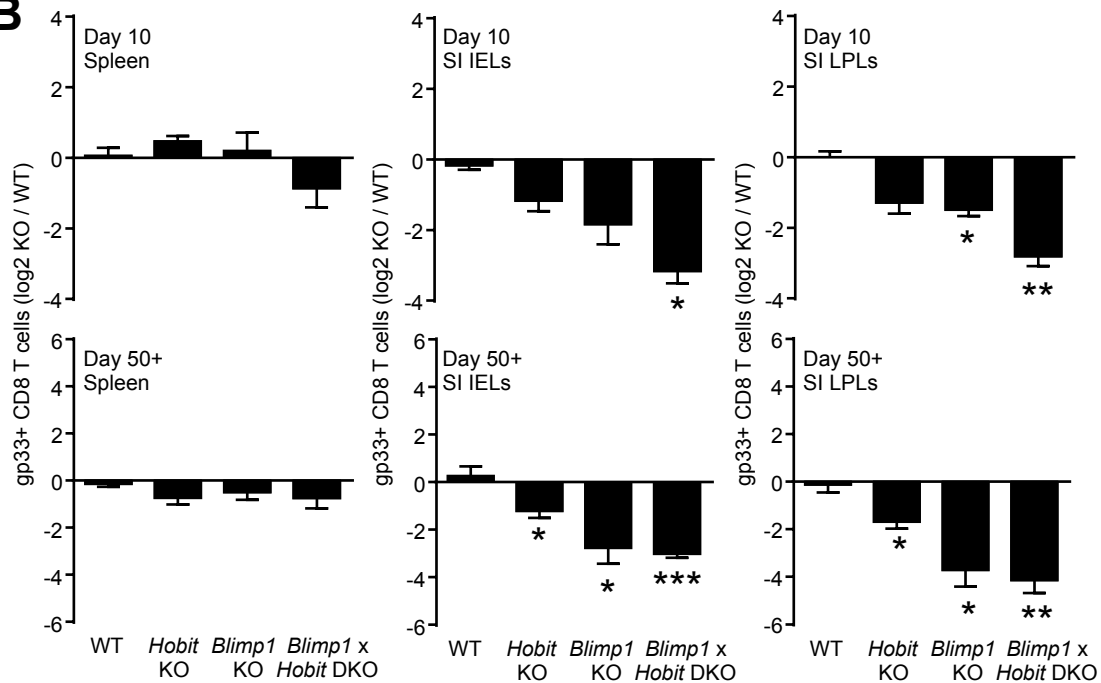
Figure S16: Hobit and Blimp1 suppress pathways of tissue-egress at the transcriptional level and promote localization of NKT cells in the red pulp of the spleen. (A-C) The expression of (A) *Klf2*, (B) *S1pr1* and (C) *Ccr7* was quantified by qPCR in splenic NKT cells of WT, *Hobit* KO, *Blimp1* KO and *Blimp1* x *Hobit* DKO mice. (D-F) NKT cells in the red pulp but not in the white pulp of the spleen were labeled by intravenous (i.v.) injection of (D,E) anti-CD44 and (F) anti-CD45 antibodies. (D) Histograms display labeling of splenic NKT cells with i.v. injected anti-CD44 within the Ly5.1+ WT compartment (black line) and the indicated Ly5.2+ WT or mutant compartments (filled grey) in mixed BM chimeric mice. (E) The ratio between the indicated Ly5.2+ and Ly5.1+ compartments of mixed BM chimeric mice was quantified for red pulp (i.v. CD44+) and white pulp (i.v. CD44-) NKT cells in spleen. (F) Numbers of splenic red pulp (i.v. CD45+) and white pulp (i.v. CD45-) NKT cells were determined in WT and *Blimp1* x *Hobit* DKO mice. (G) Spleen sections of WT (left panel) and *Blimp1* x *Hobit* DKO mice (right panel) were stained with anti-CD3 to label T cells (white), with anti-B220 to label B cells (blue) and with PBS57-loaded tetramers to label NKT cells (red). Data in (A-E) are pooled from two independent experiments with 3-6 mice per group. Data in (F) are representative of two independent experiments with three mice per group. Data in (G) represent two independent experiments. * *P* < 0.05, ** *P* < 0.01 and *** *P* < 0.001 as determined by one-way ANOVA (A-C,E) or by two-tailed Student's *t* test (F). Bars denote mean ± S.E.M.

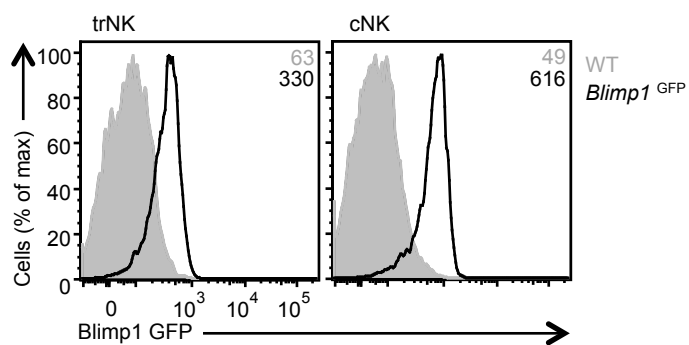
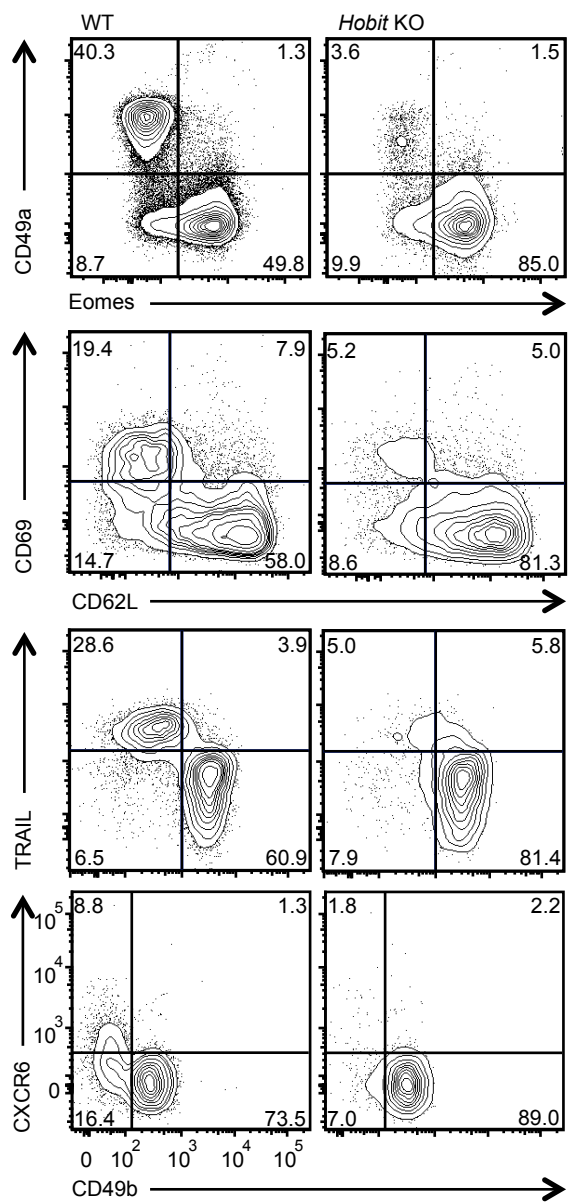
Figure S17: Hobit and Blimp1 share genome-wide binding sites. Venn diagram displays the overlap between DNA binding sites of Hobit and Blimp1 in CD8 T cells, as identified by ChIP-sequencing. Data is based on one Hobit and Blimp1 ChIP-sequencing experiment.

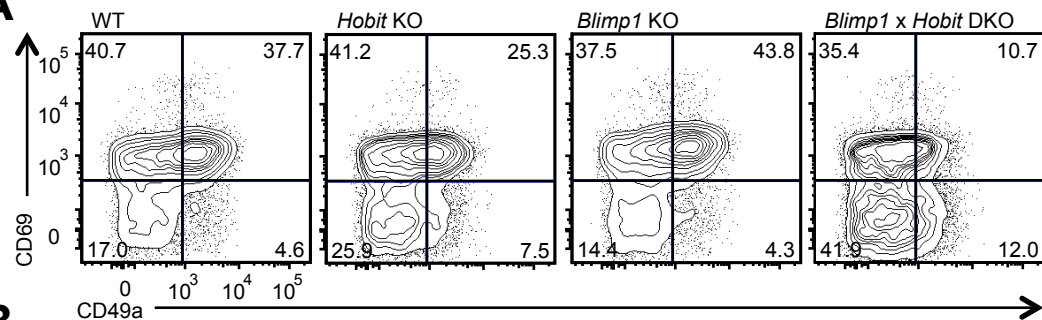
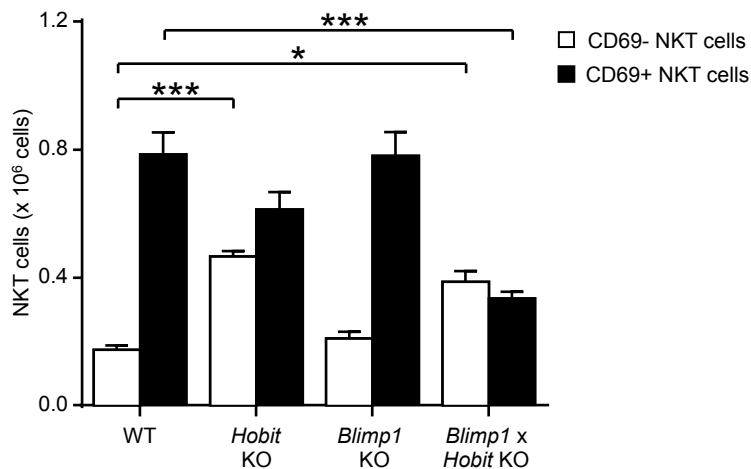
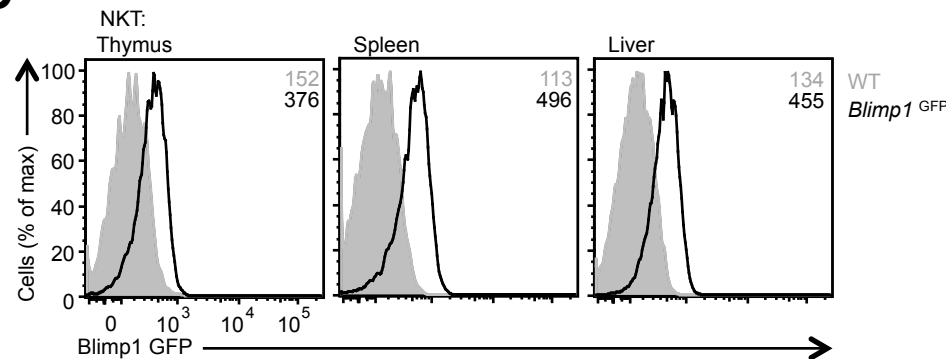
A**B****C**

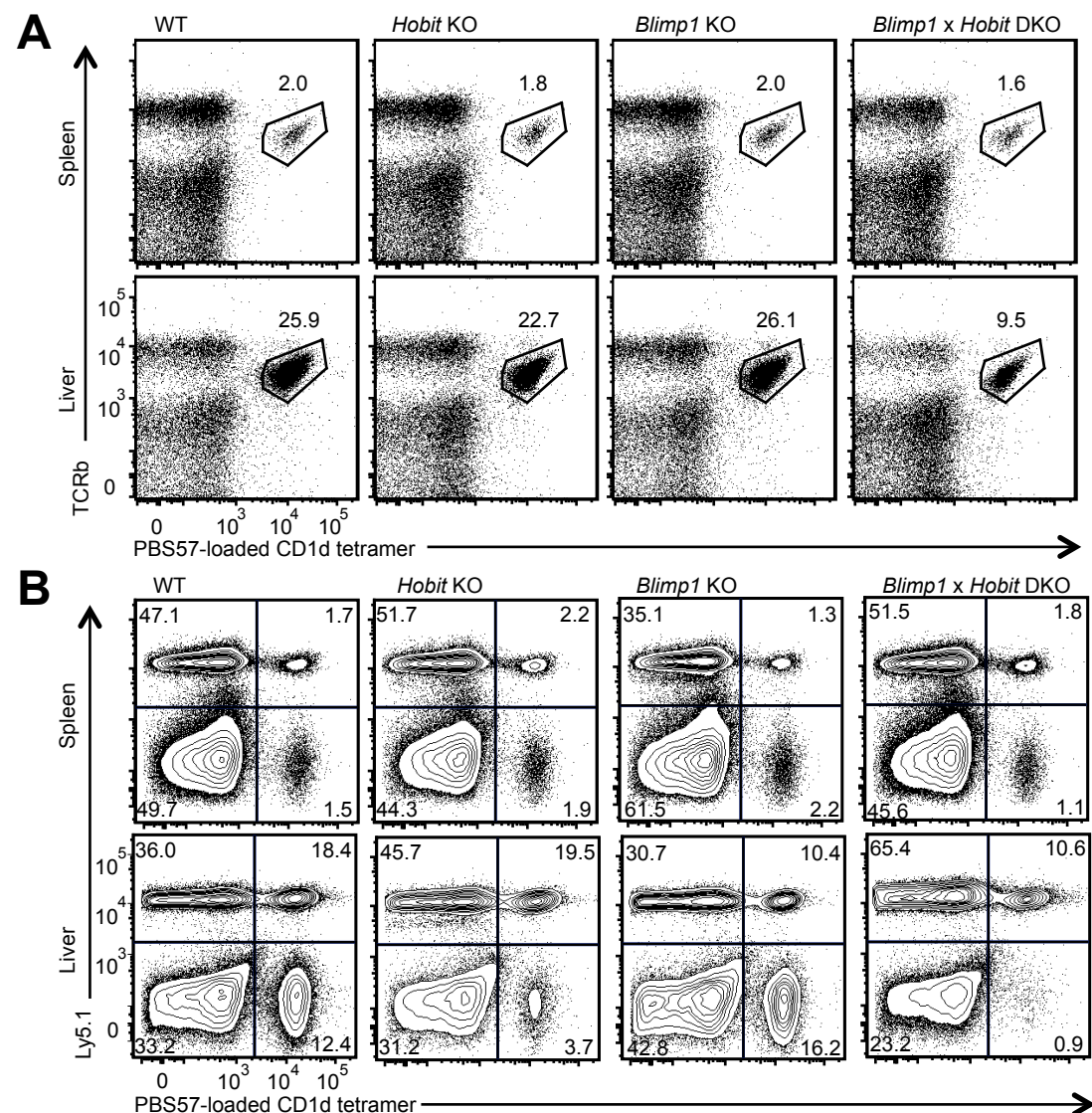
A**B**

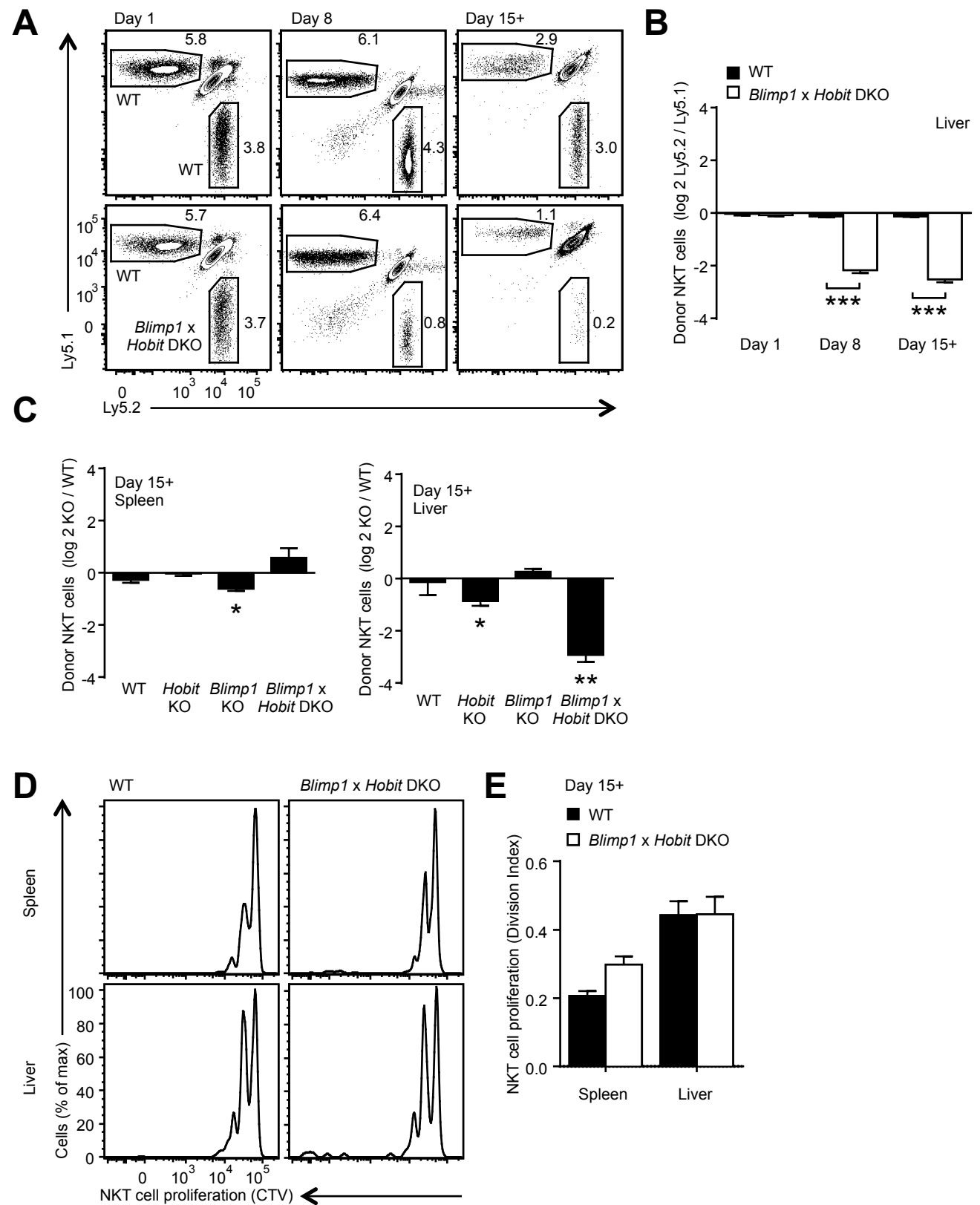
A**B****C****D****E****F****G**

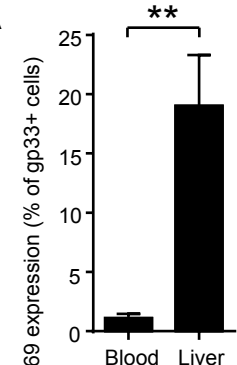
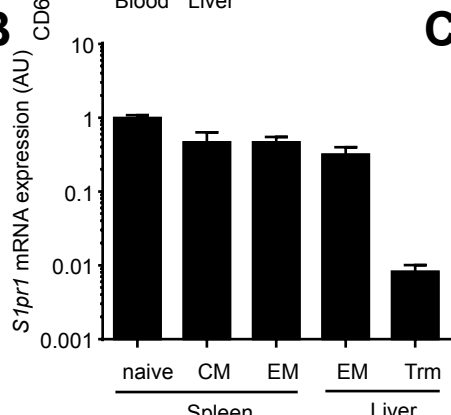
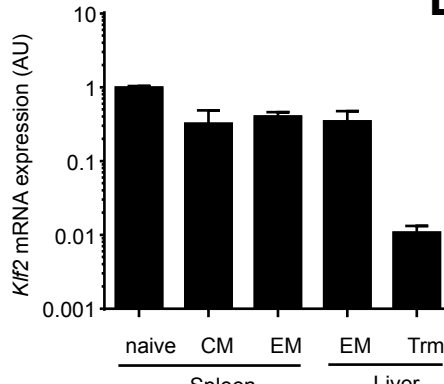
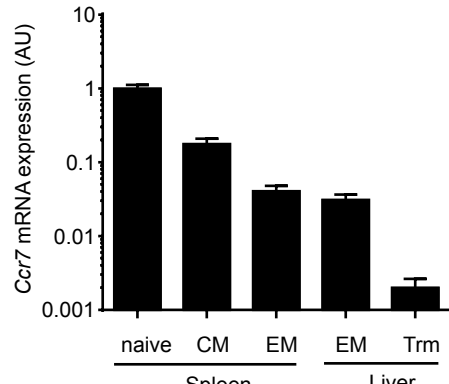
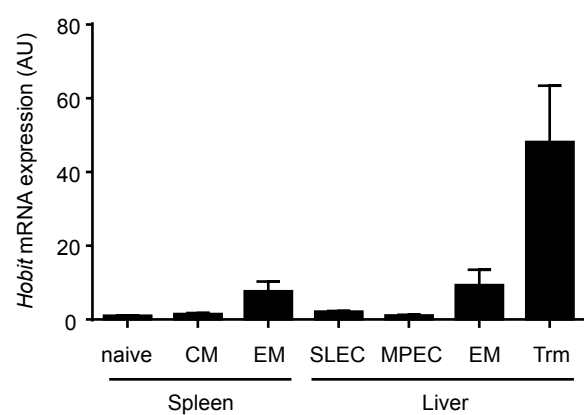
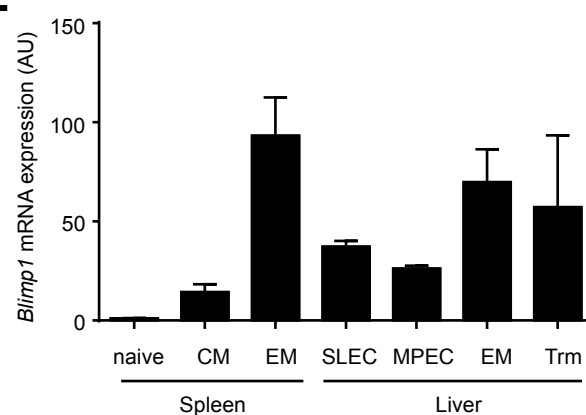
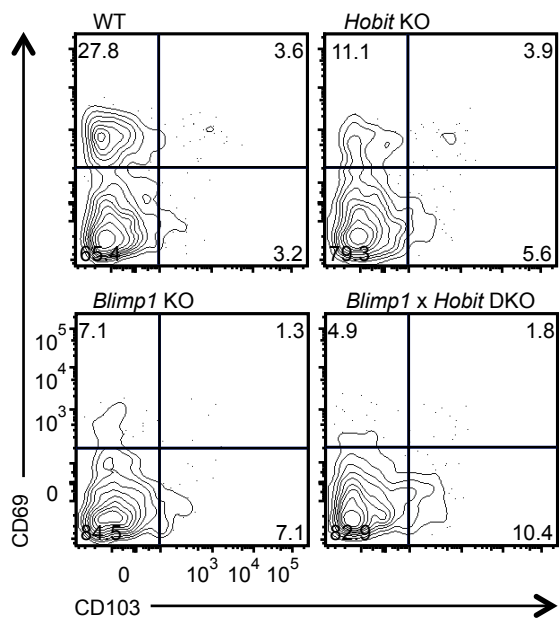
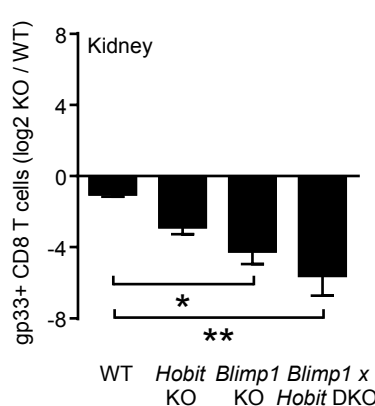
A**B**

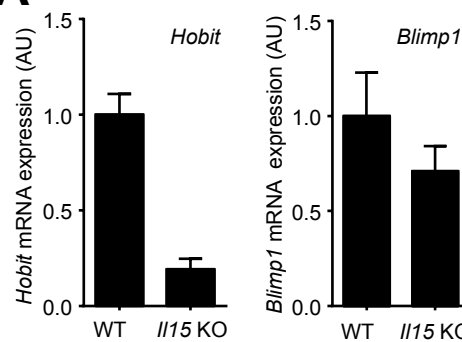
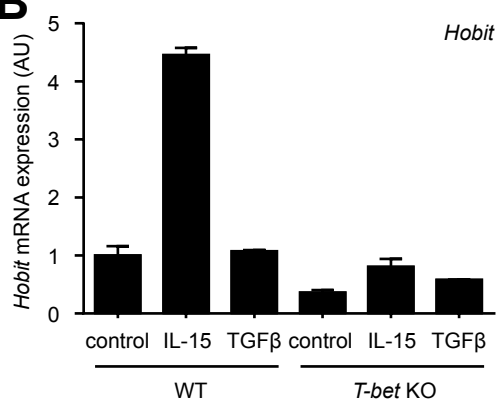
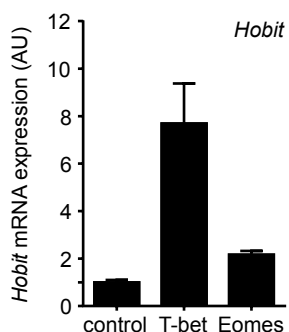
A**B**

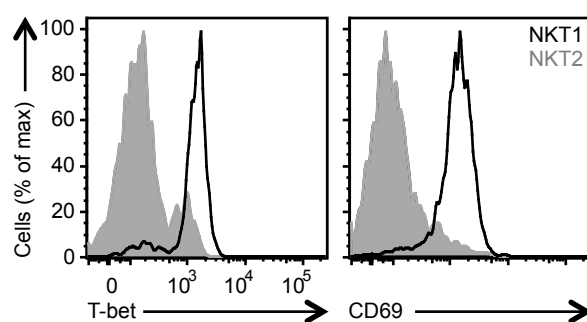
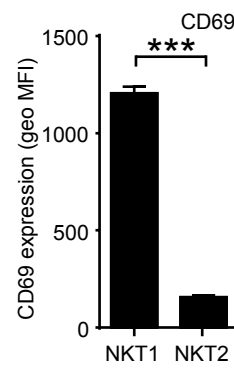
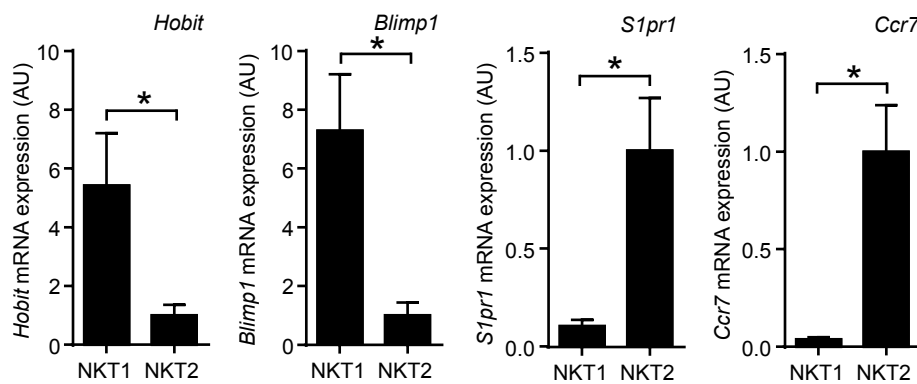
A**B****C**

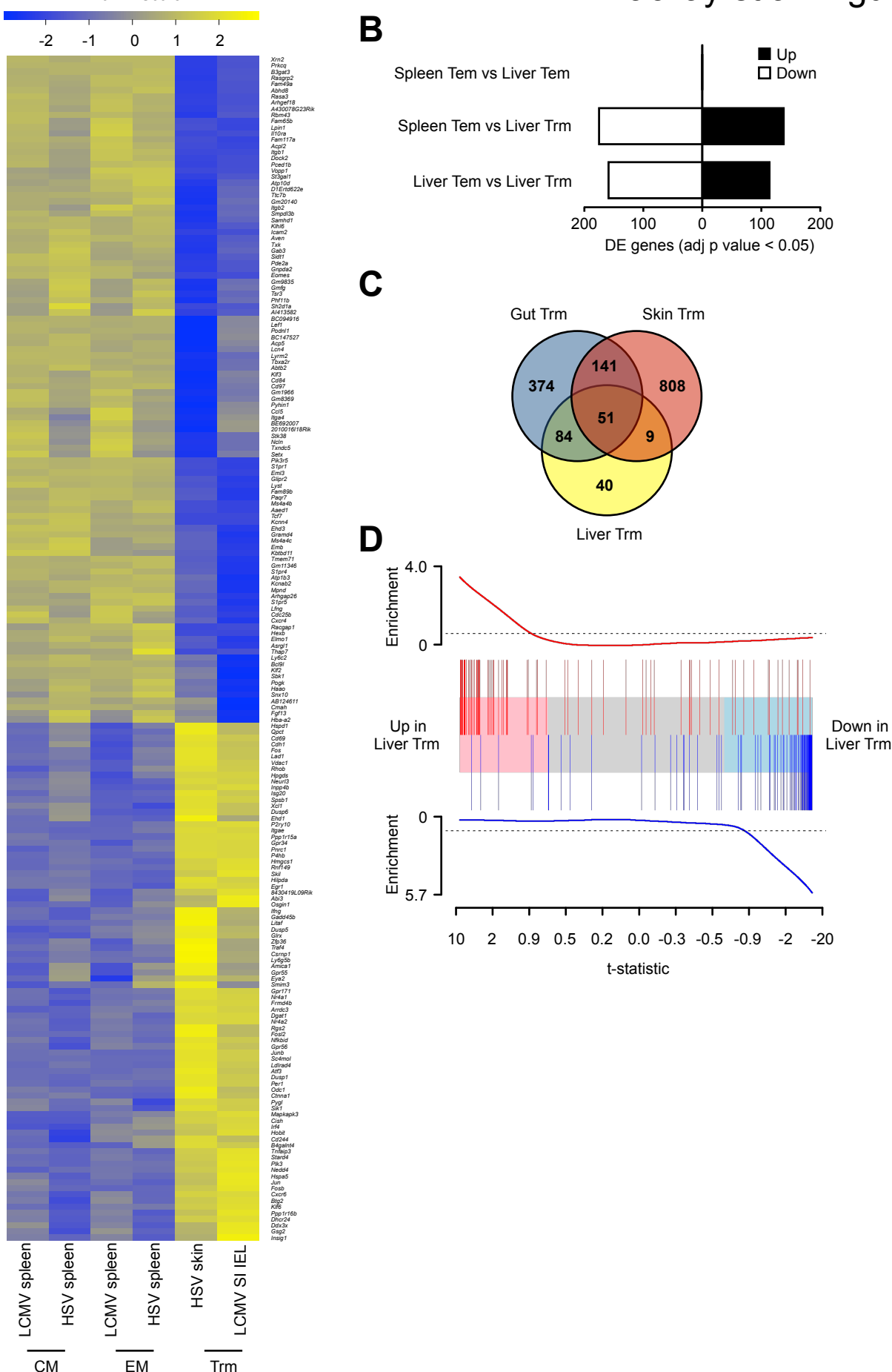


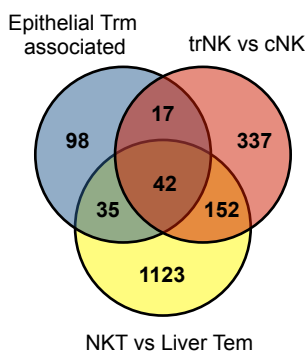
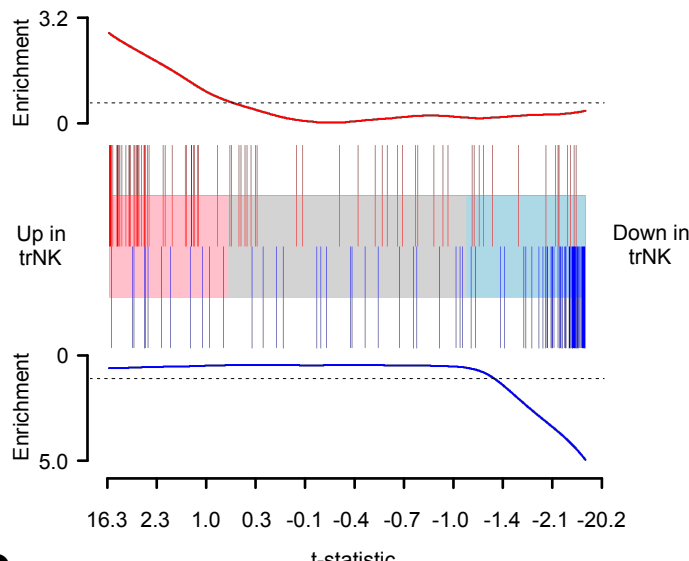
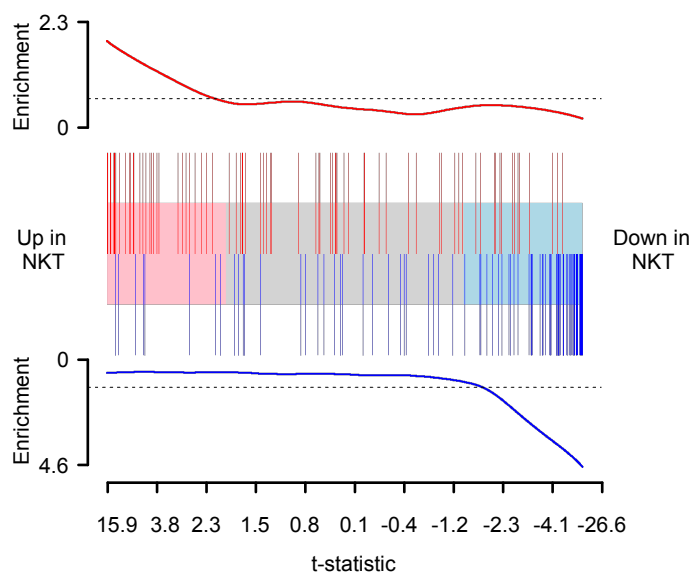


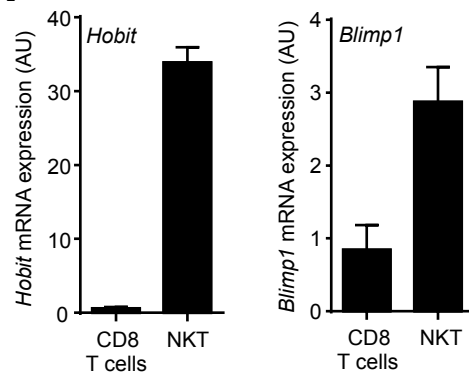
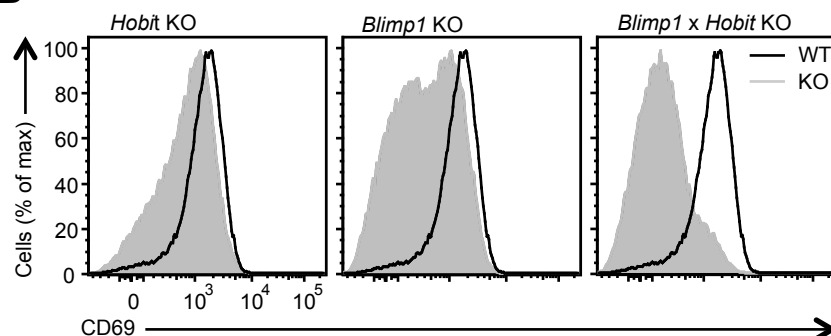
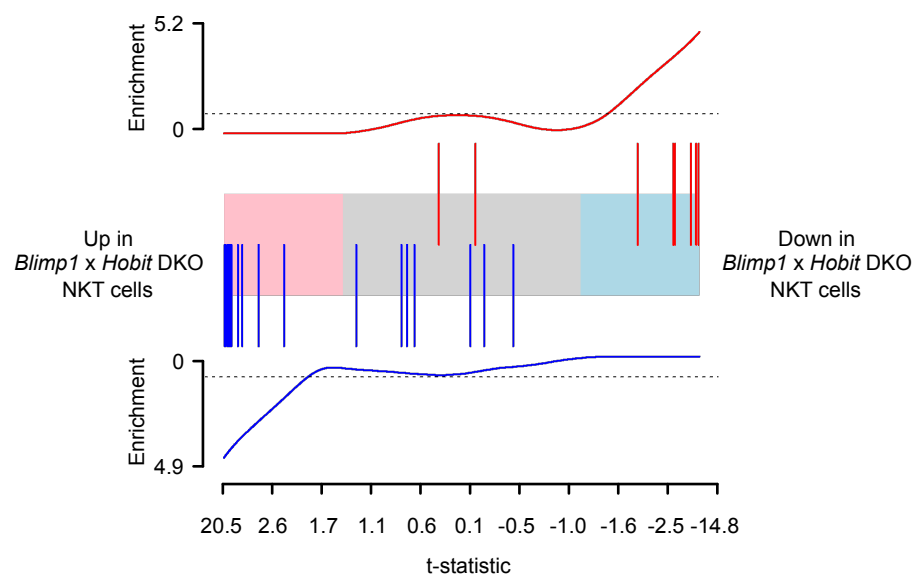
A**B****C****D****E****F****G****H**

A**B****C**

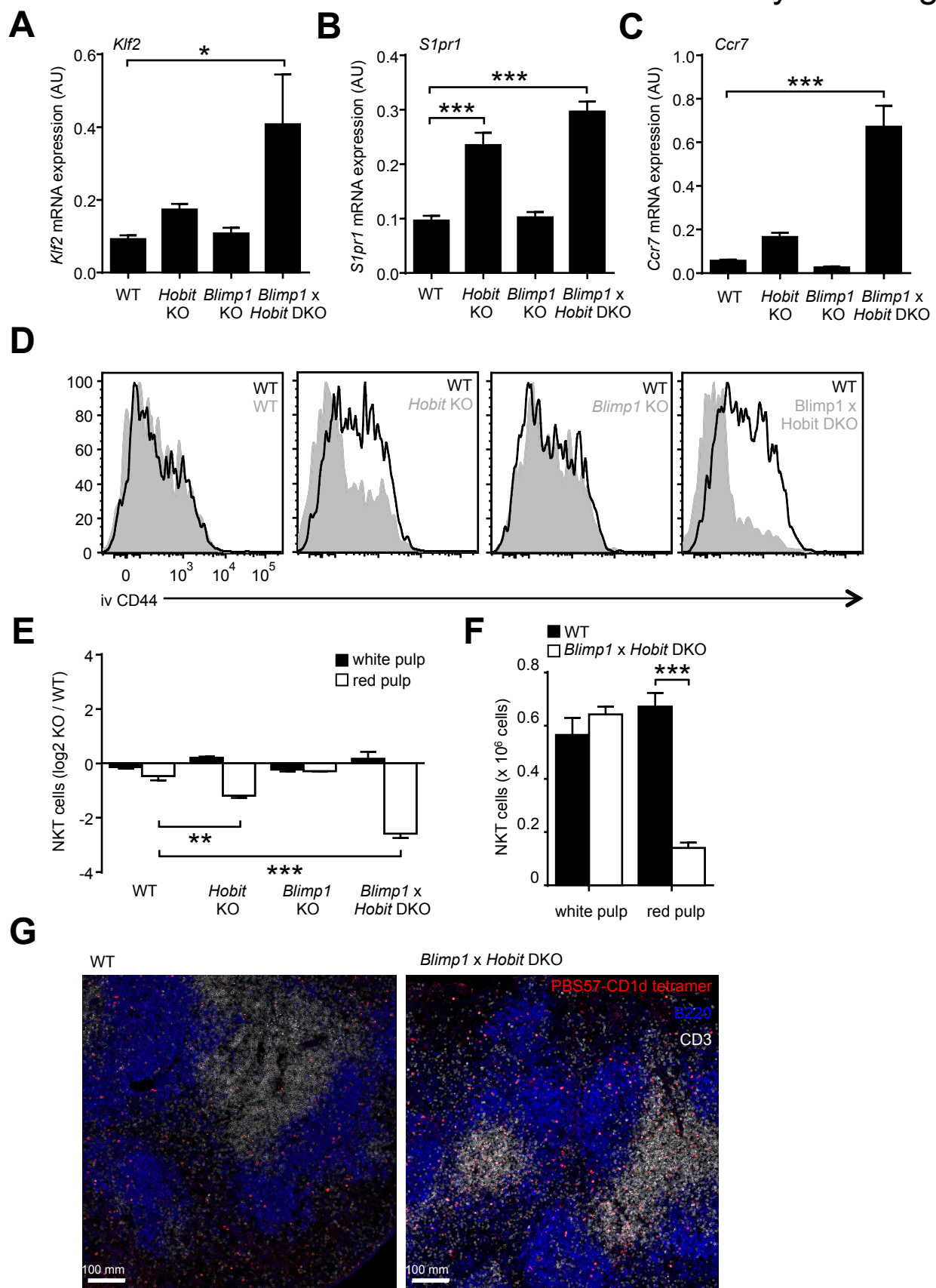
A**B****C**

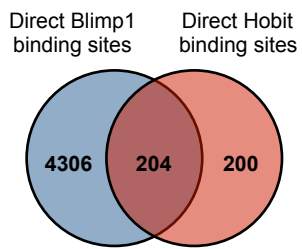


A**B****C**

A**B****C**

Mackay et al. Figure S16





References

1. L. K. Mackay, A. Rahimpour, J. Z. Ma, N. Collins, A. T. Stock, M. L. Hafon, J. Vega-Ramos, P. Lauzurica, S. N. Mueller, T. Stefanovic, D. C. Tscharke, W. R. Heath, M. Inouye, F. R. Carbone, T. Gebhardt, The developmental pathway for CD103⁺CD8⁺ tissue-resident memory T cells of skin. *Nat. Immunol.* **14**, 1294–1301 (2013). [Medline](#) [doi:10.1038/ni.2744](#)
2. K. P. van Gisbergen, N. A. Kragten, K. M. Hertoghs, F. M. Wensveen, S. Jonjic, J. Hamann, M. A. Nolte, R. A. van Lier, Mouse Hobit is a homolog of the transcriptional repressor Blimp-1 that regulates NKT cell effector differentiation. *Nat. Immunol.* **13**, 864–871 (2012). [Medline](#) [doi:10.1038/ni.2393](#)
3. A. Kallies, A. Xin, G. T. Belz, S. L. Nutt, Blimp-1 transcription factor is required for the differentiation of effector CD8(+) T cells and memory responses. *Immunity* **31**, 283–295 (2009). [Medline](#) [doi:10.1016/j.jimmuni.2009.06.021](#)
4. R. L. Rutishauser, G. A. Martins, S. Kalachikov, A. Chandele, I. A. Parish, E. Meffre, J. Jacob, K. Calame, S. M. Kaech, Transcriptional repressor Blimp-1 promotes CD8(+) T cell terminal differentiation and represses the acquisition of central memory T cell properties. *Immunity* **31**, 296–308 (2009). [Medline](#) [doi:10.1016/j.jimmuni.2009.05.014](#)
5. S. P. Berzins, F. W. McNab, C. M. Jones, M. J. Smyth, D. I. Godfrey, Long-term retention of mature NK1.1⁺ NKT cells in the thymus. *J. Immunol.* **176**, 4059–4065 (2006). [Medline](#) [doi:10.4049/jimmunol.176.7.4059](#)
6. G. Gasteiger, X. Fan, S. Dikiy, S. Y. Lee, A. Y. Rudensky, Tissue residency of innate lymphoid cells in lymphoid and nonlymphoid organs. *Science* **350**, 981–985 (2015). [Medline](#) [doi:10.1126/science.aac9593](#)
7. D. K. Sojka, B. Plougastel-Douglas, L. Yang, M. A. Pak-Wittel, M. N. Artyomov, Y. Ivanova, C. Zhong, J. M. Chase, P. B. Rothman, J. Yu, J. K. Riley, J. Zhu, Z. Tian, W. M. Yokoyama, Tissue-resident natural killer (NK) cells are cell lineages distinct from thymic and conventional splenic NK cells. *eLife* **3**, e01659 (2014). [Medline](#)
8. S. Y. Thomas, S. T. Scanlon, K. G. Griewank, M. G. Constantinides, A. K. Savage, K. A. Barr, F. Meng, A. D. Luster, A. Bendelac, PLZF induces an intravascular surveillance program mediated by long-lived LFA-1–ICAM-1 interactions. *J. Exp. Med.* **208**, 1179–1188 (2011). [Medline](#) [doi:10.1084/jem.20102630](#)
9. C. Daussy, F. Faure, K. Mayol, S. Viel, G. Gasteiger, E. Charrier, J. Bienvenu, T. Henry, E. Debien, U. A. Hasan, J. Marvel, K. Yoh, S. Takahashi, I. Prinz, S. de Bernard, L. Buffat, T. Walzer, T-bet and Eomes instruct the development of two distinct natural killer cell lineages in the liver and in the bone marrow. *J. Exp. Med.* **211**, 563–577 (2014). [Medline](#) [doi:10.1084/jem.20131560](#)
10. S. M. Gordon, J. Chaix, L. J. Rupp, J. Wu, S. Madera, J. C. Sun, T. Lindsten, S. L. Reiner, The transcription factors T-bet and Eomes control key checkpoints of natural killer cell maturation. *Immunity* **36**, 55–67 (2012). [Medline](#) [doi:10.1016/j.jimmuni.2011.11.016](#)
11. M. L. Robinette, A. Fuchs, V. S. Cortez, J. S. Lee, Y. Wang, S. K. Durum, S. Gilfillan, M. Colonna, L. Shaw, B. Yu, A. Goldrath, S. Mostafavi, A. Regev, E. Y. Kim, D. F. Dwyer,

- M. B. Brenner, K. F. Austen, A. Rhoads, D. Moodley, H. Yoshida, D. Mathis, C. Benoist, T. Nabekura, V. Lam, L. L. Lanier, B. Brown, M. Merad, V. Cremasco, S. Turley, P. Monach, M. L. Dustin, Y. Li, S. A. Shinton, R. R. Hardy, T. Shay, Y. Qi, K. Sylvia, J. Kang, K. Fairfax, G. J. Randolph, M. L. Robinette, A. Fuchs, M. Colonna; Immunological Genome Consortium, Transcriptional programs define molecular characteristics of innate lymphoid cell classes and subsets. *Nat. Immunol.* **16**, 306–317 (2015). [Medline doi:10.1038/ni.3094](#)
12. A. Kallies, S. Carotta, N. D. Huntington, N. J. Bernard, D. M. Tarlinton, M. J. Smyth, S. L. Nutt, A role for Blimp1 in the transcriptional network controlling natural killer cell maturation. *Blood* **117**, 1869–1879 (2011). [Medline doi:10.1182/blood-2010-08-303123](#)
13. E. M. Steinert, J. M. Schenkel, K. A. Fraser, L. K. Beura, L. S. Manlove, B. Z. Iggyártó, P. J. Southern, D. Masopust, Quantifying memory CD8 T cells reveals regionalization of immunosurveillance. *Cell* **161**, 737–749 (2015). [Medline doi:10.1016/j.cell.2015.03.031](#)
14. J. M. Schenkel, K. A. Fraser, D. Masopust, Cutting edge: Resident memory CD8 T cells occupy frontline niches in secondary lymphoid organs. *J. Immunol.* **192**, 2961–2964 (2014). [Medline doi:10.4049/jimmunol.1400003](#)
15. L. M. Wakim, A. Woodward-Davis, M. J. Bevan, Memory T cells persisting within the brain after local infection show functional adaptations to their tissue of residence. *Proc. Natl. Acad. Sci. U.S.A.* **107**, 17872–17879 (2010). [Medline doi:10.1073/pnas.1010201107](#)
16. L. M. Wakim, A. Woodward-Davis, R. Liu, Y. Hu, J. Villadangos, G. Smyth, M. J. Bevan, The molecular signature of tissue resident memory CD8 T cells isolated from the brain. *J. Immunol.* **189**, 3462–3471 (2012). [Medline doi:10.4049/jimmunol.1201305](#)
17. L. K. Mackay, E. Wynne-Jones, D. Freestone, D. G. Pellicci, L. A. Mielke, D. M. Newman, A. Braun, F. Masson, A. Kallies, G. T. Belz, F. R. Carbone, T-box transcription factors combine with the cytokines TGF-β and IL-15 to control tissue-resident memory T cell fate. *Immunity* **43**, 1101–1111 (2015). [Medline doi:10.1016/j.jimmuni.2015.11.008](#)
18. A. Xin, F. Masson, Y. Liao, S. Preston, T. Guan, R. Gloury, M. Olshansky, J. X. Lin, P. Li, T. P. Speed, G. K. Smyth, M. Ernst, W. J. Leonard, M. Pellegrini, S. M. Kaech, S. L. Nutt, W. Shi, G. T. Belz, A. Kallies, A molecular threshold for effector CD8(+) T cell differentiation controlled by transcription factors Blimp-1 and T-bet. *Nat. Immunol.* **17**, 422–432 (2016). [Medline doi:10.1038/ni.3410](#)
19. Y. J. Lee, K. L. Holzapfel, J. Zhu, S. C. Jameson, K. A. Hogquist, Steady-state production of IL-4 modulates immunity in mouse strains and is determined by lineage diversity of iNKT cells. *Nat. Immunol.* **14**, 1146–1154 (2013). [Medline doi:10.1038/ni.2731](#)
20. L. Gattinoni, X. S. Zhong, D. C. Palmer, Y. Ji, C. S. Hinrichs, Z. Yu, C. Wrzesinski, A. Boni, L. Cassard, L. M. Garvin, C. M. Paulos, P. Muranski, N. P. Restifo, Wnt signaling arrests effector T cell differentiation and generates CD8⁺ memory stem cells. *Nat. Med.* **15**, 808–813 (2009). [Medline doi:10.1038/nm.1982](#)
21. G. Jeannet, C. Boudousquié, N. Gardiol, J. Kang, J. Huelsken, W. Held, Essential role of the Wnt pathway effector Tcf-1 for the establishment of functional CD8 T cell memory. *Proc. Natl. Acad. Sci. U.S.A.* **107**, 9777–9782 (2010). [Medline doi:10.1073/pnas.0914127107](#)

22. X. Zhou, S. Yu, D. M. Zhao, J. T. Harty, V. P. Badovinac, H. H. Xue, Differentiation and persistence of memory CD8(+) T cells depend on T cell factor 1. *Immunity* **33**, 229–240 (2010). [Medline doi:10.1016/j.jimmuni.2010.08.002](#)
23. F. A. Vieira Braga, K. M. Hertoghs, N. A. Kragten, G. M. Doody, N. A. Barnes, E. B. Remmerswaal, C. C. Hsiao, P. D. Moerland, D. Wouters, I. A. Derkx, A. van Stijn, M. Demkes, J. Hamann, E. Eldering, M. A. Nolte, R. M. Tooze, I. J. ten Berge, K. P. van Gisbergen, R. A. van Lier, Blimp-1 homolog Hobit identifies effector-type lymphocytes in humans. *Eur. J. Immunol.* **45**, 2945–2958 (2015). [Medline doi:10.1002/eji.201545650](#)
24. S. K. Bromley, S. Y. Thomas, A. D. Luster, Chemokine receptor CCR7 guides T cell exit from peripheral tissues and entry into afferent lymphatics. *Nat. Immunol.* **6**, 895–901 (2005). [Medline doi:10.1038/ni1240](#)
25. G. F. Debes, C. N. Arnold, A. J. Young, S. Krautwald, M. Lipp, J. B. Hay, E. C. Butcher, Chemokine receptor CCR7 required for T lymphocyte exit from peripheral tissues. *Nat. Immunol.* **6**, 889–894 (2005). [Medline doi:10.1038/ni1238](#)
26. M. Minnich, H. Tagoh, P. Bönelt, E. Axelsson, M. Fischer, B. Cebolla, A. Tarakhovsky, S. L. Nutt, M. Jaritz, M. Busslinger, Multifunctional role of the transcription factor Blimp-1 in coordinating plasma cell differentiation. *Nat. Immunol.* **17**, 331–343 (2016). [Medline doi:10.1038/ni.3349](#)
27. S. Ariotti, M. A. Hogenbirk, F. E. Dijkgraaf, L. L. Visser, M. E. Hoekstra, J. Y. Song, H. Jacobs, J. B. Haanen, T. N. Schumacher, Skin-resident memory CD8⁺ T cells trigger a state of tissue-wide pathogen alert. *Science* **346**, 101–105 (2014). [Medline](#)
28. T. Gebhardt, L. M. Wakim, L. Eidsmo, P. C. Reading, W. R. Heath, F. R. Carbone, Memory T cells in nonlymphoid tissue that provide enhanced local immunity during infection with herpes simplex virus. *Nat. Immunol.* **10**, 524–530 (2009). [Medline doi:10.1038/ni.1718](#)
29. X. Jiang, R. A. Clark, L. Liu, A. J. Wagers, R. C. Fuhlbrigge, T. S. Kupper, Skin infection generates non-migratory memory CD8⁺ T(RM) cells providing global skin immunity. *Nature* **483**, 227–231 (2012). [Medline doi:10.1038/nature10851](#)
30. J. M. Schenkel, K. A. Fraser, L. K. Beura, K. E. Pauken, V. Vezys, D. Masopust, Resident memory CD8 T cells trigger protective innate and adaptive immune responses. *Science* **346**, 98–101 (2014). [Medline doi:10.1126/science.1254536](#)
31. A. Kallies, J. Hasbold, D. M. Tarlinton, W. Dietrich, L. M. Corcoran, P. D. Hodgkin, S. L. Nutt, Plasma cell ontogeny defined by quantitative changes in Blimp-1 expression. *J. Exp. Med.* **200**, 967–977 (2004). [Medline doi:10.1084/jem.20040973](#)
32. L. E. Dow, Z. Nasr, M. Saborowski, S. H. Ebbesen, E. Manchado, N. Tasdemir, T. Lee, J. Pelletier, S. W. Lowe, Conditional reverse tet-transactivator mouse strains for the efficient induction of TRE-regulated transgenes in mice. *PLOS ONE* **9**, e95236 (2014). [Medline doi:10.1371/journal.pone.0095236](#)
33. S. Finotto, M. F. Neurath, J. N. Glickman, S. Qin, H. A. Lehr, F. H. Green, K. Ackerman, K. Haley, P. R. Galle, S. J. Szabo, J. M. Drazen, G. T. De Sanctis, L. H. Glimcher, Development of spontaneous airway changes consistent with human asthma in mice lacking T-bet. *Science* **295**, 336–338 (2002). [Medline doi:10.1126/science.1065544](#)

34. M. K. Kennedy, M. Glaccum, S. N. Brown, E. A. Butz, J. L. Viney, M. Embers, N. Matsuki, K. Charrier, L. Sedger, C. R. Willis, K. Brasel, P. J. Morrissey, K. Stocking, J. C. Schuh, S. Joyce, J. J. Peschon, Reversible defects in natural killer and memory CD8 T cell lineages in interleukin 15-deficient mice. *J. Exp. Med.* **191**, 771–780 (2000). [Medline](#) [doi:10.1084/jem.191.5.771](#)
35. Y. Liao, G. K. Smyth, W. Shi, The Subread aligner: Fast, accurate and scalable read mapping by seed-and-vote. *Nucleic Acids Res.* **41**, e108 (2013). [Medline](#) [doi:10.1093/nar/gkt214](#)
36. Y. Liao, G. K. Smyth, W. Shi, featureCounts: An efficient general purpose program for assigning sequence reads to genomic features. *Bioinformatics* **30**, 923–930 (2014). [Medline](#) [doi:10.1093/bioinformatics/btt656](#)
37. C. W. Law, Y. Chen, W. Shi, G. K. Smyth, voom: Precision weights unlock linear model analysis tools for RNA-seq read counts. *Genome Biol.* **15**, R29 (2014). [Medline](#) [doi:10.1186/gb-2014-15-2-r29](#)
38. M. E. Ritchie, B. Phipson, D. Wu, Y. Hu, C. W. Law, W. Shi, G. K. Smyth, limma powers differential expression analyses for RNA-sequencing and microarray studies. *Nucleic Acids Res.* **43**, e47 (2015). [Medline](#) [doi:10.1093/nar/gkv007](#)
39. G. K. Smyth, Linear models and empirical Bayes methods for assessing differential expression in microarray experiments. *Stat. Appl. Genet. Mol. Biol.* **3**, 1–25 (2004). [Medline](#) [doi:10.2202/1544-6115.1027](#)
40. D. Wu, E. Lim, F. Vaillant, M. L. Asselin-Labat, J. E. Visvader, G. K. Smyth, ROAST: Rotation gene set tests for complex microarray experiments. *Bioinformatics* **26**, 2176–2182 (2010). [Medline](#) [doi:10.1093/bioinformatics/btq401](#)
41. A. Ebert, S. McManus, H. Tagoh, J. Medvedovic, G. Salvagiotto, M. Novatchkova, I. Tamir, A. Sommer, M. Jaritz, M. Busslinger, The distal V(H) gene cluster of the IgH locus contains distinct regulatory elements with Pax5 transcription factor-dependent activity in pro-B cells. *Immunity* **34**, 175–187 (2011). [Medline](#) [doi:10.1016/j.jimmuni.2011.02.005](#)
42. R. Revilla-i-Domingo, I. Bilic, B. Vilagos, H. Tagoh, A. Ebert, I. M. Tamir, L. Smeenk, J. Trupke, A. Sommer, M. Jaritz, M. Busslinger, The B-cell identity factor Pax5 regulates distinct transcriptional programmes in early and late B lymphopoiesis. *EMBO J.* **31**, 3130–3146 (2012). [Medline](#) [doi:10.1038/emboj.2012.155](#)
43. A. Aszódi, MULTOVL: Fast multiple overlaps of genomic regions. *Bioinformatics* **28**, 3318–3319 (2012). [Medline](#) [doi:10.1093/bioinformatics/bts607](#)
44. S. J. van Heeringen, G. J. Veenstra, GimmeMotifs: A de novo motif prediction pipeline for ChIP-sequencing experiments. *Bioinformatics* **27**, 270–271 (2011). [Medline](#) [doi:10.1093/bioinformatics/btq636](#)